

University of Texas at Tyler

Scholar Works at UT Tyler

Chemistry Theses

Chemistry

Summer 9-12-2022

EXAMINATION OF THE TIME DELAYED INDUCTION BETWEEN PRIOR ENCAPSULATION OF CATALYTIC ENZYMES IN P22 VIRUS- LIKE PARTICLES

Andrea Hernandez Irias
ahernandez29@patriots.uttyler.edu

Follow this and additional works at: https://scholarworks.uttyler.edu/chemistry_grad

 Part of the [Biochemistry Commons](#), [Biotechnology Commons](#), [Molecular Biology Commons](#), and the [Structural Biology Commons](#)

Recommended Citation

Hernandez Irias, Andrea, "EXAMINATION OF THE TIME DELAYED INDUCTION BETWEEN PRIOR ENCAPSULATION OF CATALYTIC ENZYMES IN P22 VIRUS-LIKE PARTICLES" (2022). *Chemistry Theses*. Paper 3.
<http://hdl.handle.net/10950/4063>

This Thesis is brought to you for free and open access by the Chemistry at Scholar Works at UT Tyler. It has been accepted for inclusion in Chemistry Theses by an authorized administrator of Scholar Works at UT Tyler. For more information, please contact tgullings@uttyler.edu.

EXAMINATION OF THE TIME DELAYED INDUCTION BETWEEN PRIOR
ENCAPSULATION OF CATALYTIC ENZYMES IN P22 VIRUS-LIKE PARTICLES

Andrea Hernandez Irias

A thesis submitted in partial fulfillment
of the requirements for the degree of
Master of Science in Chemistry
Department of Chemistry and Biochemistry

Dustin Patterson, Ph.D., Committee Chair

College of Arts and Sciences

The University of Texas at Tyler
Tyler, Texas

This is to certify that the Master Thesis of


ANDREA HERNANDEZ IRIAS

has been approved for the thesis requirement on
Wednesday, August 3RD, 2022
for the Master of Science in Chemistry.

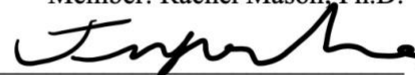
Approvals:



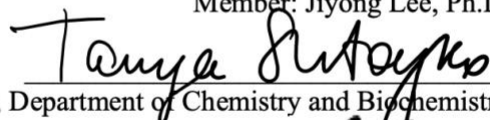
Thesis/Dissertation Chair: Dustin Patterson, Ph.D.



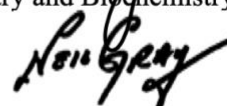
Member: Rachel Mason, Ph.D.



Member: Jiyong Lee, Ph.D.



Chair, Department of Chemistry and Biochemistry



Dean, College of Arts and Science

© Copyright 2022 by Andrea Hernandez Irias
All rights reserved.

TABLE OF CONTENTS

TABLE OF CONTENTS	4
LIST OF FIGURES	5
ACKNOWLEDGMENTS	8
I. INTRODUCTION.....	9
A. PROTEIN CAGES AS NANOCONTAINERS.	11
B. PROTEIN CAGES FAMILIES OF NANOSTRUCTURES.....	13
II. P22 BACTERIOPHAGE VIRUS-LIKE PARTICLES.....	19
A. VIRUS LIKE PARTICLES	19
B. P22 VIRUS-LIKE PARTICLES	22
C. STRUCTURE AND FOLDING OF THE COAT PROTEIN	23
D. STRUCTURE AND FOLDING OF THE SCAFFOLDING PROTEIN	24
E. ENCAPSULATION OF CATALYTIC CARGOES.....	25
III. DESIGNING METHODS FOR TEMPORAL ENCAPSULATION OF ENZYMES INSIDE OF THE P22 VLP	27
IV. MATERIALS AND METHODS.....	33
V. INVESTIGATIONS AND FINDINGS FOR 0 HOUR AND 1 HOUR ENCAPSULATION STRATEGIES	40
A. TEMPORAL INVESTIGATION OF FORMATE DEHYDROGENASE	40
B. TEMPORAL INVESTIGATION OF ALCOHOL DEHYDROGENASE D	48
VI. CONCLUSION AND FUTURE DIRECTIONS.....	55
BIBLIOGRAPHY	57

LIST OF FIGURES

Figure 1. Examples of protein cages and virus-like particles. Structures shown are as follow (A)Bacteriophage P22, (B)Ferritin, (c) Encapsulin.	10
Figure 2. Representation of Protein Cages Interfaces. (A) Cryo-electron microscopy imaging reconstruction of sulfurous turreted icosahedral virus (75 nm in diameter) isolated from a boiling, acidic environment in Yellowstone National Park. (B) Schematic illustration of the three interfaces in a protein cage available for chemical or genetic modification.	12
Figure 3. Capsid Assembly Mechanism. Three dimers from a hexamer, two of which assemble into a dodecamer, and two dodecamers assemble into the full shell. (Edwardson et al. 2022).	20
Figure 4. (a) The formation of capsid nuclei can happen spontaneously above a critical concentration or can be induced by environmental changes, as well as the interaction with the cargo. (c) The cargo can be the leading driving force to bring into proximity to rearrange into completed capsids.	22
Figure 5. (A)Bacteriophage P22 Coat Protein. (B) Bacteriophage P22 scaffolding protein	24
Figure 6. Comparison of FDH-P22 produced from either sequential or co-expressed strategies. (A) SDS-PAGE gel results of FDH-P22 produced via sequential (Seq) or co-expression (Co) methods. Both strategies showed co-purification of FDH-SP (59 kDa) and CP (47 kDa) by SDS-PAGE. (B)Transmission electron microscope images showing that both strategies produce P22 nanoparticles that are indistinguishable from one another. Scale bar are 200nm. (C)Comparison of the activity of conversion of formate to carbon dioxide simultaneously converting NAD ⁺ to NADH, by FDH-P22 generated by either sequential or co-expression methods which was monitored at 340 nm. No activity is observed for even high amounts of coFDH-P22, which only shows scattering effects due to the P22 VLP, whereas seqFDH-P22 was found to be highly active. According to Patterson et al.	30
Figure 7. Strategies for encapsulation of active formate dehydrogenase enzyme (FDH). (A) Single vector approach where Scaffolding protein (SP) is fused with FDH and co-expressed with the bacteriophage P22 VLP coat protein (CP) and inducing expression with IPTG directing encapsulation. (B) Two-vector approach that delays the CP from being expressed by fist inducing FDH-SP fused protein with arabinos, allowing time to mature, and then induced the expression of the CP with IPTG to induce encapsulation.	31
Figure 8. SDS-PAGE Characterization of FDH-P22 produce by sequential induction by using a two-plasmid system. The figure represents the SDS-PAGE analysis for the 0 and 1 hour construct. Two batches of the 0 hour construct are being represented by the lanes labeled 1 and 2.	40
Figure 9. Transmission electron microscope FDH-P22 Characterization. The TEM images of the 0 and 1 hour constructs produced using a two-plasmid approached. The 0 hour construct show abnormal formation of the FDH-P22.	41
Figure 10. Characterization of FDH P22 construct by SEC-MALS/2ELS/RI. SEC chromatograms for FDH-P22 produce with two plasmid system providing the 0 and 1 hour constructs.	42
Figure 11. Evaluation of FDH-P22 kinetics with variation of formate concentration. Plots showing the results of kinetics assays from FDH-P22 produced with 1 hour delay. Data is fit to a Michaelis-Menten equation.	43

Figure 12. Evaluation of Candida Boidinni FDH control kinetics analyzed through a variation of formate concentrations. The plot was produced through the analysis of industrially produced FDH and purchased from Sigma Aldrich.....	44
Figure 13. Evaluation of Kinetics of FDH-SP produced in the presence of an empty pRSFDuet plasmid.....	47
Figure 14. Comparison of FDH activity per enzyme encapsulated inside the P22 VLP by sequential induction. Enzyme activity per enzyme encapsulated showed no significant change between induction times of FDH-SP. The enzyme activity per enzyme encapsulated was by dividing the average K_{cat} by the average number of enzymes encapsulated for 3 batches produced. Error bars indicate the standard deviation found for each data set.	48
Figure 15. SDS-PAGE Characterization of AdhD P22. The 0 and 1 hour samples showed poor separation, which has been seen for AdhD-SP and CP in previous studies. SEC-MAL/RI helped further confirmation of AdhD-SP was encapsulated in the P22 VLP	49
Figure 16. Characterization of seqAdhD-P22 by transmission electron microscopy. TEM images of seqAdhD-P22 produced with 0 and 1 hour delays. TEM samples are compared to previous studies performed by the Patterson research group.....	50
Figure 17. Evaluation of AdhD-P22 kinetics with variations of Acetoin concentrations. Plots showing the kinetics assays for AdhD-P22 produced with 0, and 1 delay between AdhD-SP and CP induction.....	52
Figure 18. Comparison of AdhD activity per enzyme encapsulated inside the P22 VLP by sequential induction. Enzyme activity per enzyme encapsulated, found by dividing the average K_{cat} by the average number of enzymes encapsulated in a total of three batches produced, was not observed to change significantly between induction times of AdhD-SP.....	54

LIST OF TABLES

Table 1. Determination of FDH-P22 VLP molar mass, packaging, and solution radii analysis by SEC-MALS/QELS/RI. Increased copies of FDH were observed with increased induction times of FD-SP, maintaining overall packaging of teh interior as evidenced by the Rg/Rh. Single vector co-induced FDH-P22 showed the highest packaging, with the longest sequential expression stratechy showing comparable packaging levels of FDH. The table shows previoys data from 2 to 16 hours before encapsulation, and the 0 to 1 hour of this study.	43
Table 2. The results show the average apparent kinetic parameters. Three independent preparations for FDH-P22 produced via co-expression, sequential expression (0 hr, 1 hr, 2 hr, 4 hr, and 16 hr) and encapsulation strategies, as well as non-encapsulated FDH	45
Table 3. Determination of AdhD-P22 VLP molar mass, packaging, and solution radii analysis by SEC-MALS/QELS/RI. Increased copies of AdhD were observed with increased induction times of AdhD-SP.....	51
Table 4. Kinetic parameters determined for AdhD-P22 constructs. The results show the apparent kinetic parameters for AdhD-P22 produced via sequential expression and a comparison with past values obtained from the co-expression strategies, in vivo encapsulation, and the non-encapsulated AdhD-SP (free Adhd-SP) values with *indicate statistical difference (Student t-test $p < 0.05$) vs 2, 4, and 16 hour seqAdhD-P22 samples.....	53

ACKNOWLEDGMENTS

This might be the most important section of my thesis. I would like to acknowledge that this work would not be possible if God was not part of the life of every person involved in this research and program. He granted eternal patience, open hearts, and opportunities during times that I did not see it possible and placed special people at every step of the way. For that reason, I would like to acknowledge those who were not only my mentors, but also those who helped me grow through these two years.

I would like to acknowledge and give thanks to my principal investigator, Dr. Dustin Patterson, whose endless patience made this work possible. I would also like to thank my committee members, Dr. Rachel Mason and Dr. Jiyong Lee.

To my parents, Ana and Oscar, a special thanks for their encouragement and support through the years. For their sacrifices, mentorship, and reassurance. To my siblings, Oscar, and Alexandra, for their endless inspiration, amusement, and reinforcement. Without their support I would not have been able to be here.

To my college friends, Sarah, Bre, Caleb, Katie, Adrian and Jerome for adventuring in this master's journey with me, asking for updates, and encouraging me to finish. To my friends Betsy and Loren for their love and support through these two years, and a special thanks to Elliott for helping me focus on the future, and for being one of the most caring and loving human beings on this planet.

Finally, an especial and eternal thanks to the entire Chemistry and Biochemistry Department for teaching and mentoring me for years and even a pandemic. There will never be enough words in both the entire English and Spanish language that could express my gratitude. This department was an answer to prayer, a blessing in my life during a time when I didn't know I needed it. Thank you for all your help.

I. INTRODUCTION

Protein cages are compartments derived from protein subunits that self-assemble into hollow structures with nano-sized internal space surrounded by a protein coat. Protein cages have been found in a host of biological systems and have a range of biologic functions, from iron storage containers like ferritins, found in humans, to the capsids that form the structural foundation of viruses (Cristie-David et al. 2018). The unique structure of protein cages and their size has garnered much attention for their use in a number of materials applications (Liu et al. 2018). In addition to their natural structures, the genetic encoding and protein composition confer the ability to readily modify protein cage structures through bioengineering techniques that maintain their robust self-assembly, solubility, and biocompatibility properties, but allow for synthetic enhancements and chemical reprogramming (Edwardson et al. 2022). Their programable interfaces permit the application of protein cages to a broad range of nanomaterials and the development of new nanobiotechnology (Beyeh et al. 2018). Examples of protein cage structures, including virus-like particles (VLPs), which are protein cages derived from viral capsids, are shown in **Figure 1**.

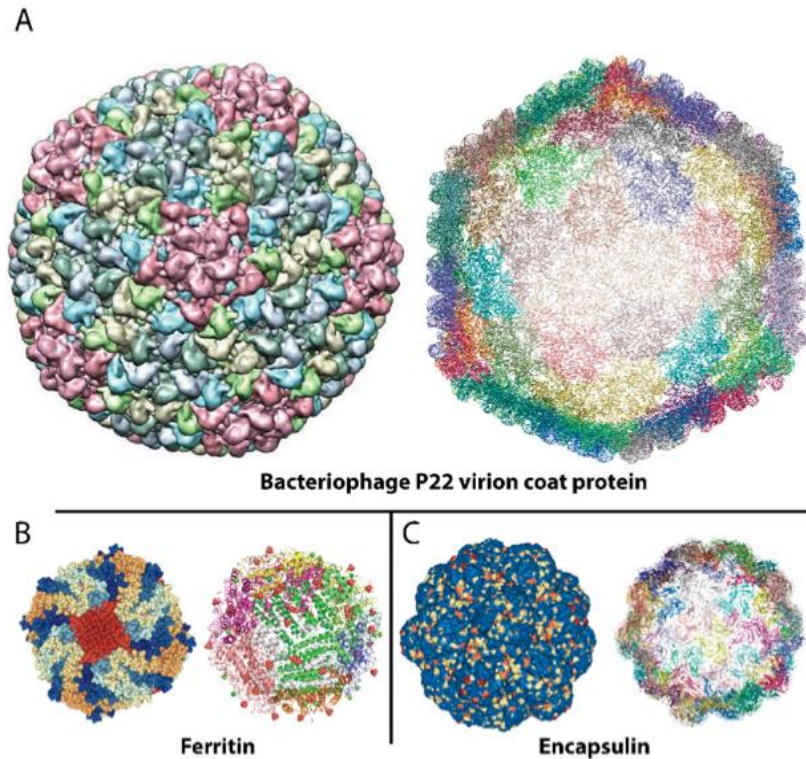


Figure 1. Examples of protein cages and virus-like particles. Structures shown are as follow (A)Bacteriophage P22, (B)Ferritin, (c) Encapsulin.

Protein cage assembly and formation can be performed either *in vivo*, by assembly of purified proteins outside of the cell in a test tube, or *in vitro*, whereby the assembly takes place in the cell, typically as the protein subunits are being produced in their host cell (Giessen and Silver 2016). In recent years, synthetic biochemists have harnessed both genetic and synthetic chemical methods to manipulate protein cage structures both *in vitro* and *in vivo* (Casini et al. 2004). Protein cages have been produced from a number of expression host cells, however expression of protein subunits for protein cages is typically carried out in bacteria, such as *E. coli*, or yeast, since these production systems can easily be scaled up and are cost-effective (Fuenmayor et al. 2017). The diversity of production systems and *in vitro/in vivo* methods for assembly provide broad adaptability of protein cages for different applications, such as therapeutic delivery,

vaccines, and containers for medical applications that require more stringent care to prevent contamination or unwanted immune responses (Terasaka et al. 2018). A wide range of protein cages are in existence, many have been fully characterized to the molecular level, and they contain a range of shapes, sizes, and molecular architectures that provide a “library” of possible protein cages to choose from in developing new designer protein cage nanomaterials (Beyeh et al. 2018). A key feature of protein cages is the hollow interior, in which guest molecules/macromolecules can be trapped and confined. A large body of research has been dedicated to the encapsulation of various guest molecules on the interior of protein cage, which is discussed in the next section.

A. Protein cages as Nanocontainers.

Protein cages present an inspirational structure due to its sustainability, ease of production, as well as the profound need of biocompatible materials in medicine, technology, and energy applications (Kim et al. 2019). In the past decade, scientific interaction with protein cages have been highly focused on therapeutic applications. (Heddle et al. 2017). Use of protein cages can be subcategorized into either *biotemplates* or *biomimics* depending on the use of the protein cages. Biotemplates consist of biologic nanoparticles equipped to form novel and functional building materials (Freeman 2017) while *biomimics* intend to recreate or closely resemble the biological function of a protein or proteins structure (Ganganboina and Doong 2018). One of the main uses protein cages have been studied for is their utilization as nanocontainers. The directed assembly of viral capsids through single protein structures are viewed as molecular Lego sets, since they are usually assembling from repeating protein designs. They form highly symmetrical structures, as stated previously, from helical, icosahedral, cubic, or tetrahedral symmetries. In nature, structure drives function, the variety of structures present display the variability of

protein cages from viral capsids, which are adapted to their various environments (Lua et al. 2014). However, protein cages are cost-efficient production of proteins. They are commonly assembled from a limited number of subunits to form the robust nanostructures present in nature (Cannon et al. 2020). Protein cages present a moldable nanoplatform that can provide humanity control over the size, the shape, the biocompatibility, and the ability to change the structure and therefore the functionality by environmental stimulus (Yang et al. 2021).

Nevertheless, a single protein cannot achieve the complexity presented by the everchanging requirements for various applications, thus a “library” of proteins has been studied and their process of assembly, structural formation, and dynamics in order to harness their potential for future applications. Protein cages can form spherical, robust nanocontainers, as well as nanotubes (Schwarz et al. 2015). They can also be modified through the different interactions (**Figure 2**), such as internal interactions, surface interactions, and between the protein interfaces (Uchida et al. 2018). The variation of proteins that can be utilized can therefore provide possible control over the size, position, orientation, and synthesis of the nanocontainers.

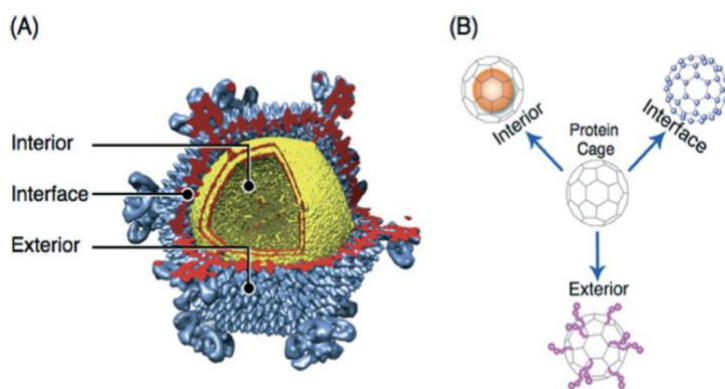


Figure 2. Representation of Protein Cages Interfaces. (A) Cryo-electron microscopy imaging reconstruction of sulfurous turreted icosahedral virus (75 nm in diameter) isolated from a boiling, acidic environment in Yellowstone National Park. (B) Schematic illustration of the three interfaces in a protein cage available for chemical or genetic modification.

Protein cages can range between 12 to 100 nanometers, and as imaginable as they are in the human mind, they are large molecular structures with a prospective chemical and genetical manipulation (Slocik et al. 2013). Since these structures are defined by their internal cargo capacity, they serve an ideal encapsulation potential for desirable nanomaterials or molecular cargos (Collett et al. 2021). Through the understanding of their assembly, protein cages can encapsule desired molecules through their directed assembly and attachment of the molecules to the interior (Edwardson et al. 2022)

The focus of the research discussed in this thesis is on the utilization of the VLP protein cage derived from the *Salmonella typhimurium* bacteriophage P22, which will be referred to as a VLP going forward, for the encapsulation of enzymes to produce protein cage nanoreactors (Kim et al. 2019). However, there are many other unique protein cages and VLP systems that have been extensively studied and are noteworthy for understanding the field. (Selivanovitch et al. 2019). The remainder of this chapter will discuss the different major families of protein cages and VLPs examined to date with a focus on their assembly, maturation, and methods for encapsulation of enzymes on their interior for constructing nanoreactors.

B. Protein Cages Families of Nanostructures

Ferritins are a family of proteins present in biological system with the main function of storing and sequestering iron (Sano et al. 2005). They are found in all domains of life and due to their function of storing inorganic iron molecules, these were the first protein cages to be used as a template for synthesis of inorganic nanoparticles. Ferritin has been classified the main iron

storage molecule available. As a nanoparticle, ferritin has been extended beyond the scope of iron storage and aims to become a functional and novel biomolecule used for medical process such as iron delivery, chemotherapy, contrast agents, and biomarkers in a number of neurological diseases (Chiou and Connor 2018). These particles are referred as ferritin-like particles. In recent approaches, ferritins-like particles have been developed to disassemble in the presence of low pH and reassemble at near neutral pH in the presence of a magnetic resonance imaging (MRI) contrast agent (Chakraborti et al. 2019), as delivery nanoparticles to induce an antigen-specific immune response (Han et al. 2014), and as protein fusions to fluorescent proteins to pave the way for new nanotechnical and pharmacological applications (Tetter and Hilvert 2017).

Encapsulins are a novel prokaryotic compartment (Gabashvili et al. 2020) composed of shell proteins that form icosahedral capsid nano compartments that are used to encapsulate only one type of cargo. Genes which produce encapsulin are present throughout prokaryotic genomes and provide a large diversity of cargo proteins. Encapsulins have been studied as well to produce programmable nanoreactors and produce nanomaterials (Ren et al. 2019; Almeida et al. 2021). Encapsulins impose a protection against proteases, such as trypsin, and maintain their robust protein structure from degradation. Studies have encouraged scientists to study encapsulins for applications in recombinant protein vaccines, treatment for cancer, and various other diseases. Additionally, they can sustain high temperature over a wide of pH range, can be engineered to alter shell cargo proteins, while enclosing enzymatic reactions, and size-constrained metal biomineralization (Sigmund et al. 2018).

Lumazine synthase are capsid-forming bacterial enzymes, which catalyzes the penultimate step in the biosynthesis of riboflavin, also known as vitamin B2 (Azuma et al. 2017). Usually forming icosahedral capsid with triangulation number of $T=1$, with an outer diameter of around 16 nm and consist of a total 60 identical subunits (Wei et al. 2017). Since mammals are dependent on the uptake of this vitamin, the production pathway is present mostly in microorganisms and plants, which establishes the lumazine synthase as an interesting protein to study for medical and vaccine development (Ra et al. 2014; Tuan et al. 2014). Studies have also shown how robust and versatile the lumazine synthase structure is by creating negatively charged luminal surfaces to investigate structural catalysts (Azuma et al. 2016). Since it is predominantly present in plants and microorganisms, including human pathogens, it is also a potential targeting nanostructure to anti-infective agents (Morgunova et al. 2007).

Major Vault Proteins, also known as ribonucleoprotein particles, are a large, oval ribonucleoprotein. They are abundant in eukaryotic cells and appear to be involved in the complex pathways of growth and proliferations of cells (Tanaka and Tsukihara 2012). Past studies have suggested that the formation, abundance, and conservation of vault proteins can have important attributes in fighting infections, resisting chemotherapy, and surviving nutritional stress, since they seem to be crucial for the dendritic cell differentiation and maturation (Suprenant 2002). In the past, they have been used to study genes associated with lung multidrug resistance and chemotherapy resistance lung cancer (Ben et al. 2019), as well as the study of an extracellular vesicle to investigate the distribution, accumulation and efflux of chemotherapeutics for breast cancer cells *in vitro* (Lehuédé et al. 2019). More importantly, and related to this research they have been utilized to encapsulate magnetic resonance imaging

contrast agents, as a promising protein structure as they are responsive to external stimuli such as heat, pH, magnetic field, etc. (Wang et al. 2015)

Heat Shock Proteins are a family of molecular chaperones which have a role in protein folding. Ranging between 10 to 150 kDa weight that are activated to detect and control different forms of stress, and an indication birds to adapt to stress changes in their environment. (Baykalir and Simsek 2018). Heat shock proteins have a highly versatile cage-like structure whose exterior and interior surfaces are modifiable to both genetic and chemical modifications. Assembling into an empty 24 subunit cage with octahedral symmetry, forming an interior diameter of 12 nm. Previously, heat shock proteins have been used to deliver tumor microenvironment targeting nanoparticles and therapeutics, such as antigens and MRI image fluorescent molecules, (Shi et al. 2020).

Viral Capsids are also a family of protein cages that are present in viral biology. The interior surface of viral capsids can direct the attachment or nucleation of molecular materials, as it does for the viral capsid in nature. Viruses package their viral genome or nucleic acid within the capsid, the mechanism for packaging the viral genome can be utilized to direct the encapsulation of non-viral genomic cargos. Nanoparticles derived from viral capsids are known as virus-like particles (VLPs). Initial VLP work focused on utilizing Cowpea chlorotic mottle virus (CCMV), an RNA-containing plant virus, which was composed by 180 identical coat protein that would then self-assemble to form an icosahedral cage structure (Minten et al. 2009). CCMV forms a structure with a 28 nm outer diameter and a 24 nm interior diameter. Currently, through protein design and genetic engineering, it is possible to apply changes in the interior structures of the

coat proteins to attach molecules that can then be encapsulated. Additional VLPs from Porcine Circovirus type 3 (PCV3) VLP with a 10 nm diameter has been developed in order to detect and facilitate the screening of swine serum for clinical purposes (Wang et al. 2020); human parvovirus B19 VLP and the effects of pH and ionic strength on the assembly process (Sánchez-Rodríguez et al. 2012); and the capsid of human papillomavirus (HPV) which accommodates multiple mutant particles natural design in order to produce an HPV vaccine for multiple strains of the virus (Wang et al. 2020).

On top of that, the employment of enzymes as biocatalyst across industries such as food processing, medical diagnostics, energy, and biofuel will require the optimized and stable enzymes. VLPs have been used in the past to encapsulate enzymes in order to stabilize them, protect them, and study them through scaffolding protein-mediated encapsulation, osmolyte-mediated encapsulation (Fu et al. 2018; Glasgow et al. 2012). The MS2 bacteriophage VLP has been used to encapsulate single-stranded-DNA in a variety of sized ranging from 200 to 1500 nucleotides. As well as encapsulating MRI contrasting enhancement molecules, proteins, and nanoparticles. Capitalizing on the 2 nm pores which allow small molecules have access to the internal VLP space (Glasgow et al. 2012; Giessen and Silver 2016). The Q β VLP has been used to encapsulate small-ultra red fluorescent proteins to generate non-invasive in vivo image agents (Fabian et al. 2020), as well as encapsulating fluorescent particles in order to bioconjugate encapsulated biomaterials. The P22 VLP has showed to have a higher encapsulation efficiency than the Q β and the MS2 (Glasgow et al. 2012), as it is assembled through the co-expression of two simple protein structures; coat protein (CP), and a scaffolding protein (SP) which directs the assembly of the capsid. The P22 VLP consist of 420 copies of the CP monomer whose assembly

is guided with the aid of approximately 300 SP. The P22 VLP has been used in the past as a programmable targeting agent, delivery nanoplatfrom, and nanoreactor platform for catalytic enzyme encapsulation. P22 provides a platform that can be modified due to the guided assembly of the scaffolding protein (SP), since the SP can be truncated, providing increased space for cargo on the interior, and will still guide the formation of the viral capsid. Moreover, the fusion of the proteins together can guarantee co-encapsulation of a defined ratio of enzyme cargoes that can be determined to determine the local concentration of encapsulated catalyst (Patterson et al. 2012; Schwarz et al. 2015; Kim et al. 2019).

II. P22 BACTERIOPHAGE VIRUS-LIKE PARTICLES

A. Virus Like Particles

Viruses have developed a large variety of capsids to packages, protect, and deliver their DNA or RNA genome (Terasaka et al. 2018). Their well-characterized 3D structure makes them a wide-ranging building block for applications (Wilkerson et al. 2018). Despite the vast differences in symmetry, shape and complexity, protein capsids follow a few common design principles (Cannon et al. 2020). Most common viral capsids studied are built to form virus-like particles (VLPs), which are viral capsid proteins that self-assemble to form the viral coat proteins produced through recombinant technology yielding a non-infectious particle (Hortsch and Weuster-Botz 2011). VLPs can be modified either through a chemical or genetic modification to provide different applications in the biotechnological realm (Lu et al. 2022). VLPs can be modified externally to produce attachment points with antigens to result in an immunological response and can be used to produce vaccines. VLPs can be modified internally to attach desirable cargos such as therapeutics, inorganic materials, catalysts, functional proteins and imagine agents (Ren et al. 2019; Patterson et al. 2012; McCoy et al. 2018).

VLPs use a symmetric arrangement of the same protein to maximize space for cargo while minimizing genetic information load and liability. Viruses have maximized arrangements of asymmetric protein chains to form triangular faces of at least three protein chains resulting in platonic solid structures such as tetrahedra, octahedra, and icosahedral, composed of four, eight, and 20 equilateral triangles, respectively (Cheng-Chung Lee et al. 2003). Icosahedral symmetric capsids are the most common natural capsids (Prevelige et al. 1988). Nature favors the icosahedral capsid since it provides a maximized container volume and making it a dominating

reaction chamber. (Edwardson et al. 2022). A curious observation, demonstrated by Caspar and Klung, of many cages consisting of more than 60 subunits, product of a single protein chain monomer, would allow small deformations in inter-subunit interactions to allow a single protein to use the same surface chemistry to create a large icosahedral symmetric capsid (Johnson and Olson 2021).

Understanding the assembly, interaction, and disassembly of protein capsids, as well as the interaction with the cargo molecule permits the scientific community to harness the system for biotechnology, nanomaterials, and applications. While some small cargos can be infused through the porous VLP surface, larger cargos might present a more difficult task that requires control over the production and assembly for the loading and, if necessary, the release of the cargo. To aid in loading large cargoes an understanding of the capsid assembly through its guided pathway to form the final complex structure with a high predictability and efficiently is needed.

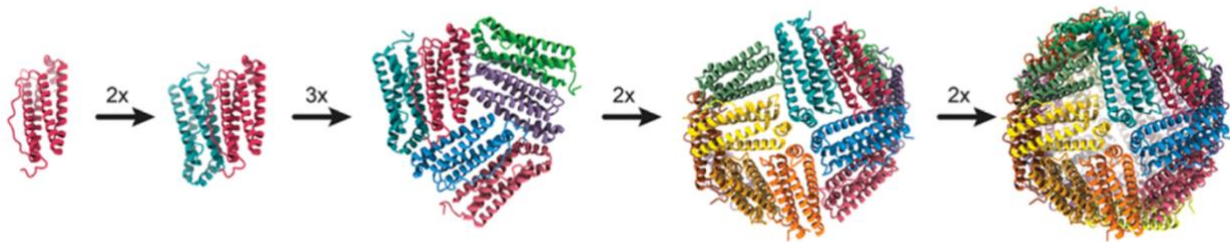


Figure 3. Capsid Assembly Mechanism. Three dimers from a hexamer, two of which assemble into a dodecamer, and two dodecamers assemble into the full shell. (Edwardson et al. 2022)

The environment in which these capsids are being formed provide a drive, since typically capsid assembly is driven by entropically stable pathways. The capsid is formed by burying its

hydrophobic surface and exposing hydrophilic surface (Gast et al. 2021). The adhesive and cohesive properties of water and the interaction water molecules have with the single protein chain leads to the formation of the capsid assembly (Johnson and Olson 2021). Yet, capsids that constitute of 24 or more subunits, rely on more than just the driving force of hydrophobic and hydrophilic interactions in solution (Le et al. 2019). They rely on quasi-equivalence and flexibility of the subunit formation. As presented in **Figure 3**, there are two extremes of the observed mechanism in which can start through nucleation-and-growth or by *en masse* (in a group) assembly around the cargo to rearrange into a well-organized capsid (Edwardson et al. 2022).

Nucleation-and-growth mechanism has most observed in capsids modeled after viruses in the presence of a low loading cargo or genomic cargo. Initially producing protomer building blocks such as dimers or trimers with low affinity to each other (Lauria et al. 2017). This allows them to associate once a critical concentration has been produced. Then they recruit additional protomers to complete the capsid assembly as depicted in **Figure 4**. *En masse* nucleation is induced by the interaction changes with environmental promoters (Calcines-Cruz et al. 2021). This can be through environmental changes cues or association with molecules such as RNA genomes or partner proteins, such as scaffolding proteins. This mechanism needs to be excellently regulated to avoid the formation of incomplete or unwanted structures. Natural systems manage this formation of unwanted structures by exploiting the weak protomer interactions, this prevents the depletion of free subunits and can reverse the binding. (Prevelige et al. 1993; Terasaka et al. 2018; Edwardson et al. 2022)

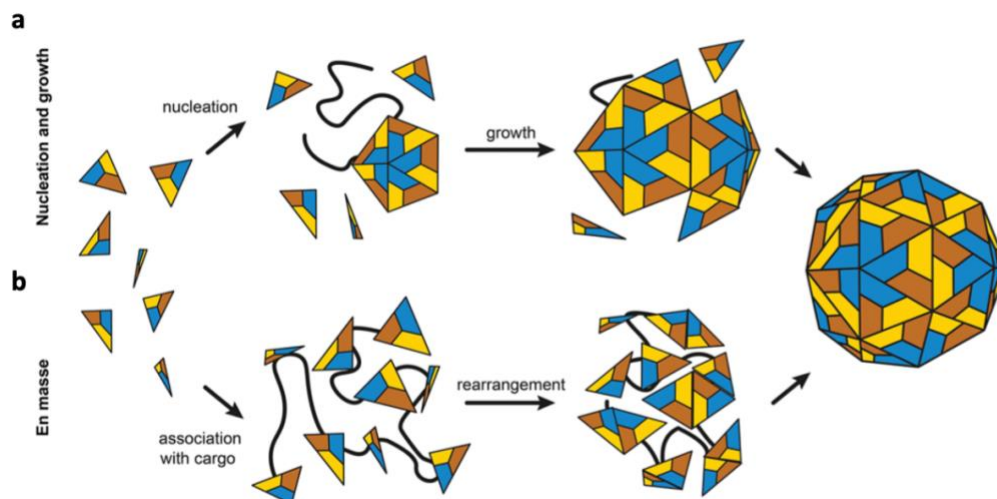


Figure 4. (a) The formation of capsid nuclei can happen spontaneously above a critical concentration or can be induced by environmental changes, as well as the interaction with the cargo. (c) The cargo can be the leading driving force to bring into proximity to rearrange into completed capsids.

B. P22 Virus-Like Particles

VLPs serve as a well-understood molecular platform without the infectious material presented in their viral counterparts. They have a regular and programable architectures derived from viruses and are an exceptional platform to develop nanomaterials. Studies on VLPs have highlighted the ability to encapsulate cargo just like their viral counterparts, although they permit greater access to a wider variety of cargo molecules (Waghvani et al. 2020)

The P22 VLP is inspired by the P22 bacteriophage in the *Podoviridae* family that infects *Salmonella typhimurium*. The assembly of the capsid requires the coat protein (CP) and scaffolding protein (SP) (**Figure 5**). In the absence of the scaffolding protein, the coat protein assembles to form a large and closed structure. This leads to the understanding of the proper folding and determination of the SP since it is necessary for the formation of the capsid;

approximately 300 copies of the 33 kDa SP co-assemble with the 420 copies of the 47 kDa CP to form a T=7 procapsid. The procapsid has structural spaces or pores, approximately 25 nm in diameter, which is located at the center of each hexameric CP cluster and provide an exit and entry port to the interior of the VLP, allowing compounds in the range of 5-8kDa entering the VLP. (Schwarz et al. 2015; Teschke and Parent 2010).

C. Structure and Folding of the Coat Protein

The P22 VLP coat protein (CP) has a unique biochemical property, which allows it to remain stable until reaching excess temperatures of 80 °C (Teschke and Parent 2010). As stated earlier, the coat protein on its own cannot produce a mature phage structure without the aid of the SP but will assemble into a T=4 capsid and have aberrant spiral structures. A mature P22 VLP capsid with a T=7 icosahedra structure will result in a 10-15% increase in volume (Parent et al. 2010). The CP assembly of the P22 VLP is simplified due to 1) the monomeric coat protein added one at a time; and 2) the maturation does not require proteolytic cleavage of the coat protein, the breakdown of the coat protein with the aid of a secondary enzyme, as some other viral capsids require (Genes et al. 1973). The icosahedral cage structure can also be utilized as a platform for modification of the exterior surface (Newcomer et al. 2015). It has been shown that amines, carboxylic acids, and thiol groups can react with activated small molecules, such as activated fluorescence labeling, without disrupting the overall cage structure (Servid et al. 2013).

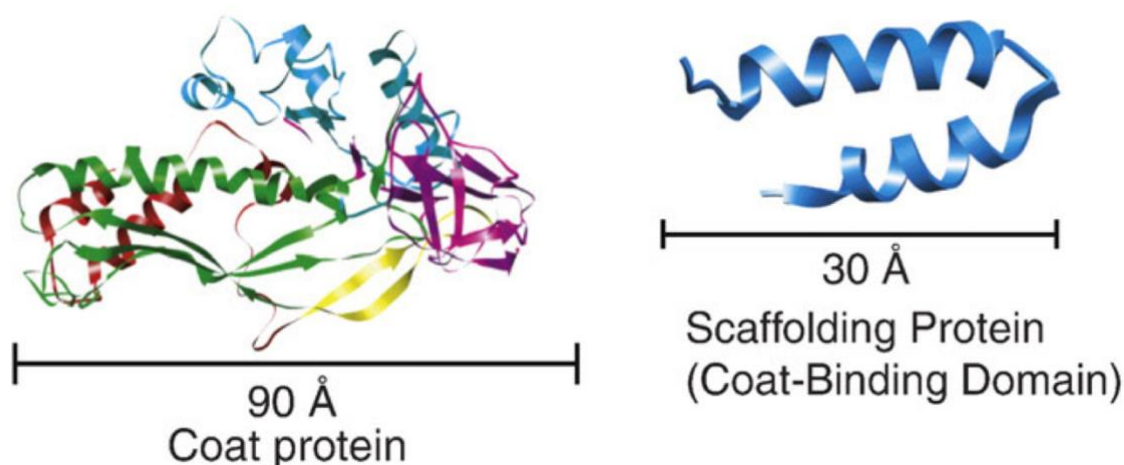


Figure 5. (A) *Bacteriophage P22 Coat Protein*. (B) *Bacteriophage P22 scaffolding protein*

D. Structure and Folding of the Scaffolding Protein

The P22 VLP scaffolding protein was predicted to be a highly α -helical protein, 33 kDa in size. The C-terminal region of the scaffolding protein compromises the part of the region that interacts with the coat protein, and the deletion of the final 11 amino acids of the SP C-terminus makes the scaffolding protein incapable of binding to the coat protein. The N-terminus on the other hand can be readily truncated and truncation by deletion of the first 141 amino acids residues of the SP is still capable to direct the assembly of the P22 VLP. The C-terminal 35 residues are revealed to be the coat binding domain. Importantly, the assembly requires the presence of CP and the SP, without a change of pH or divalent cation alteration. (Thuman-Commike et al. 1996; Johnson and Chiu 2007)

It has been previously showed by Douglas and co-workers (Waghvani et al. 2020; O’Neil et al. 2011; Uchida et al. 2018; McCoy et al. 2018), that the SP can be severely truncated at the N-terminus to up to 162 amino acid residues and still direct the assembly of the P22 VLP. The

truncated version of the SP results in additional space in the interior of the VLP (Prevelige et al. 1988). The additional empty space can be exploited to encapsulate large guest molecules/macromolecules by fusing their peptide sequence to the SP, which directs and localizes cargoes into the P22 VLP as the CP assembles. Through this strategy, it has been shown that a wide array of proteins can be encapsulated inside the P22 VLP, including the encapsulation of catalytic enzymes that remain active (Selivanovitch et al. 2021; Waghvani et al. 2020; Uchida et al. 2015; Patterson et al. 2017; O'Neil et al. 2011). The P22 VLP permits access to the encapsulated catalyst through the porous VLP surface, which contains pores of 2 to 4.5 nanometers depending on the structural morphology (Selivanovitch et al. 2021). Through the expression of the SP fused with the catalyst, high internal packaging that resemble the concentrations present in biological systems can be achieved.

E. Encapsulation of Catalytic Cargoes

Catalytic cargoes can be introduced through a series of paths explored in the past. The methods to encapsulate cargos can be divided into *in vivo* and *in vitro* strategies. The *in vitro* assembly approach grants control over an additional level of complexity than *in vivo*, but requires additional steps of purification and preparation (Waghvani et al. 2020). Additionally, the P22 VLPs produced through *in vitro* assembly can be layered to produce architectural structures that can disassemble and reassembly *in vitro*. Sharma and coworkers were able to encapsulate catalytic cargo by fusing it to the N-terminus of the truncated SP and were expressed in E.coli cells, and through a separate construct, the CP was expressed in E.coli same was done for the expression of a wild type of the CP. While the catalytic cargo-SP and the wild type SP are mixed together through different molar ratios, and a 1:1 SP:CP ratio. (Sharma and Douglas

2020). Through *in vivo* process, it is possible to attach a cargo on the VLP surface both internally and externally due to the VLP P22 repetitive protein structure. The gene encoding the CP protein can be mutated in order to permit an attachment target, not internally and externally (Giessen and Silver 2016; Azuma et al. 2018). In the past this has been allowed by mutating one amino acid into a cysteine such as S133C or K118C, and then a cargo molecule is conjugated through thiol-maleimide conjugation inside the VLP (Kim et al. 2019). This methodology was first used by tagging fluorescence labeling molecules in the interior of VLPs.

In addition, *in vivo* modifications can be directed through fusion of a catalytic enzyme to the SP, by truncating the SP and adding gene encoding information through a genetic containing an enzyme of interest, such as formate dehydrogenase (FDH), alcohol dehydrogenase D (AdhD), CelB, GalA, hydrogenase, as well as simultaneous encapsulation of multiple enzymes, to name a few (O'Neil et al. 2011). The P22 VLP provides a mechanism to encapsulate the enzyme by forming an enzyme-SP which directs the assembly of the P22 VLP in the presence of the CP. This permits the truncated SP fused with the desired enzyme to be encapsulated. (Jordan et al. 2016). Changes to enzymes kinetics have been found through the *in vivo* assembly pathway verses the normal kinetics of the enzymes and recent kinetics results have also found changes to *in vitro* encapsulated enzymes vs. their *in vivo* counterparts. Because of these differences, methods for investigating how *in vivo* encapsulation might alter enzyme kinetics are needed, which is the focus of the research outlined in the subsequent sections of this thesis.

III. DESIGNING METHODS FOR TEMPORAL ENCAPSULATION OF ENZYMES INSIDE OF THE P22 VLP

Encapsulating enzymes in the P22 VLP has been extensively studied, with one of the end goals of the research being to produce catalytic nanoreactors that protect the enzymes from denaturation and degradation. Additionally, it was hypothesized that encapsulation would lead to emergent properties and could be used to study enzymes in a crowded and confined environment that mimics cellular conditions normally experienced by enzymes. As noted in the previous chapter the P22 VLP has been utilized to encapsulate a number of different enzyme cargoes, however these have largely focused on the encapsulation of enzymes originating from hyperthermophilic organism, such as *Pyrococcus furiosus*, which are known to be robust and show more thermal and chemical stability than enzymes originating from mesophilic organisms. The advantage of encapsulating enzymes inside of VLPs is hypothesized to be more advantageous for mesophilic enzymes, but the use of the P22 VLP for mesophilic enzyme encapsulation has only recently been examined.

Encapsulation strategies of enzymes inside of the P22 VLP have largely focused on *in vivo* assembly strategies, where enzymes genetically fused to the SP are simultaneously co-expressed with the P22 CP, leading to subsequent encapsulation of the enzyme-SP fusion protein inside the P22 VLP interior. Interestingly, encapsulation of enzymes using a simultaneous co-expression strategy has resulted in active enzymes, but often with alterations to their kinetics parameters relative unencapsulated enzyme. The first example of encapsulation was examined for the hyperthermophilic alcohol dehydrogenase D (AdhD) from *P. furiosus*, which showed decreased k_{cat} and K_M upon encapsulation. The change in AdhD parameters were attributed to crowding and confinement effects at the time, since the internal concentrations of AdhD neared 6 mM, similar

to the macromolecular concentrations of the cell (Patterson, D. P et al 2012). Later examples of hyperthermophilic enzymes showed little change to the overall kinetics although co-confinement of enzymes was found to show channeling effects (Patterson, D. P et al 2014). The first example of a mesophilic enzyme encapsulated inside P22 was the encapsulation of a heme dependent cytochrome P450 (CYP) enzyme that was able to activate pro-drug after encapsulation. Interestingly, the authors utilized a two-plasmid approach for the production of the CYP for encapsulation inside the P22 VLP to obtain active enzyme. Later, Paul Jordan, et al. produced a hydrogenase enzyme using the two-plasmid approach, although induction was performed simultaneously by controlling concentrations of inducers (Jordan et al. 2016). Although the single co-expression simultaneous expression and two plasmid approach was described for the encapsulation of mesophilic enzymes, no study was performed to examine what effect these different approaches had on the overall activity of the encapsulated enzymes but focused on whether active enzyme was obtained. The previous studies have left unanswered questions into what role the encapsulation strategy, either a single vector co-induction or a multiple vector expression strategy had on enzyme kinetics.

The Patterson research group became interested in the encapsulation of a mesophilic enzyme called Formate Dehydrogenase (FDH) from *Candida boidinii*, which catalyzes both the oxidation of formate to CO₂ when it is in the presence of excess NAD⁺ and can also catalyze the reduction of CO₂ to formate with the excess concentration of NADH. Industrially FDH is used as a means of production of NADH and has also been used to produce *tert*-L-leucine, one of the largest enzymatic processes in pharmaceutical chemistry. Initially it was thought that FDH encapsulation would be useful in constructing nanoreactors that could be used in performing

carbon fixation of carbon dioxide, by FDH conversion of carbon dioxide to formate, coupled with a secondary enzymatic alcohol dehydrogenase that would yield methanol. However, initial investigations of FDH encapsulation by the single plasmid co-expression method yielded P22 VLPs encapsulating FDH that were inactive. This led to investigations with a two plasmid approach where the expression of the FDH-SP fusion protein could be staggered relative the expression of the CP. **Figure 6** shows the comparison of FDH-SP containing P22 VLPs (FDH-P22) that were prepared by two different method, simultaneous co-expression of FDH-SP and CP from a single plasmid and a staggered sequential expression of FDH-SP, followed by expression of CP from two separate plasmids. Interestingly, when the staggered expression approach, whereby FDH-SP was induced to express first for 2 hours, then subsequently CP was expressed for 2 hours, the FDH-P22 VLPs showed active FDH. These results suggested that a temporally controlled expression of FDH, and potentially other enzymes, was important to obtaining active FDH-VLPs, which spurred the investigations discussed in the remainder of this thesis.

The initial findings that FDH could only be encapsulated as an active enzyme inside the P22 VLP if FDH-SP was expressed and produced before the P22 CP suggested that the FDH-SP fusion protein need a period for maturation, which we define as protein folding and incorporation of any non-protein cofactor, before encapsulation by CP. It has been previously suggested that encapsulation of enzyme-SP fusion proteins by CP is rapid (Patterson et al. 2013). However, inactivity could also be the result of crowding inside the FDH-P22 VLP. In order to investigate the cause of the inactivity via the co-expression system and the ability to obtain active enzymes

via a two vector sequential system, the Patterson group developed an expression system strategy allowing FDH-SP, as well as other enzyme-SP systems, to be temporally expressed separate

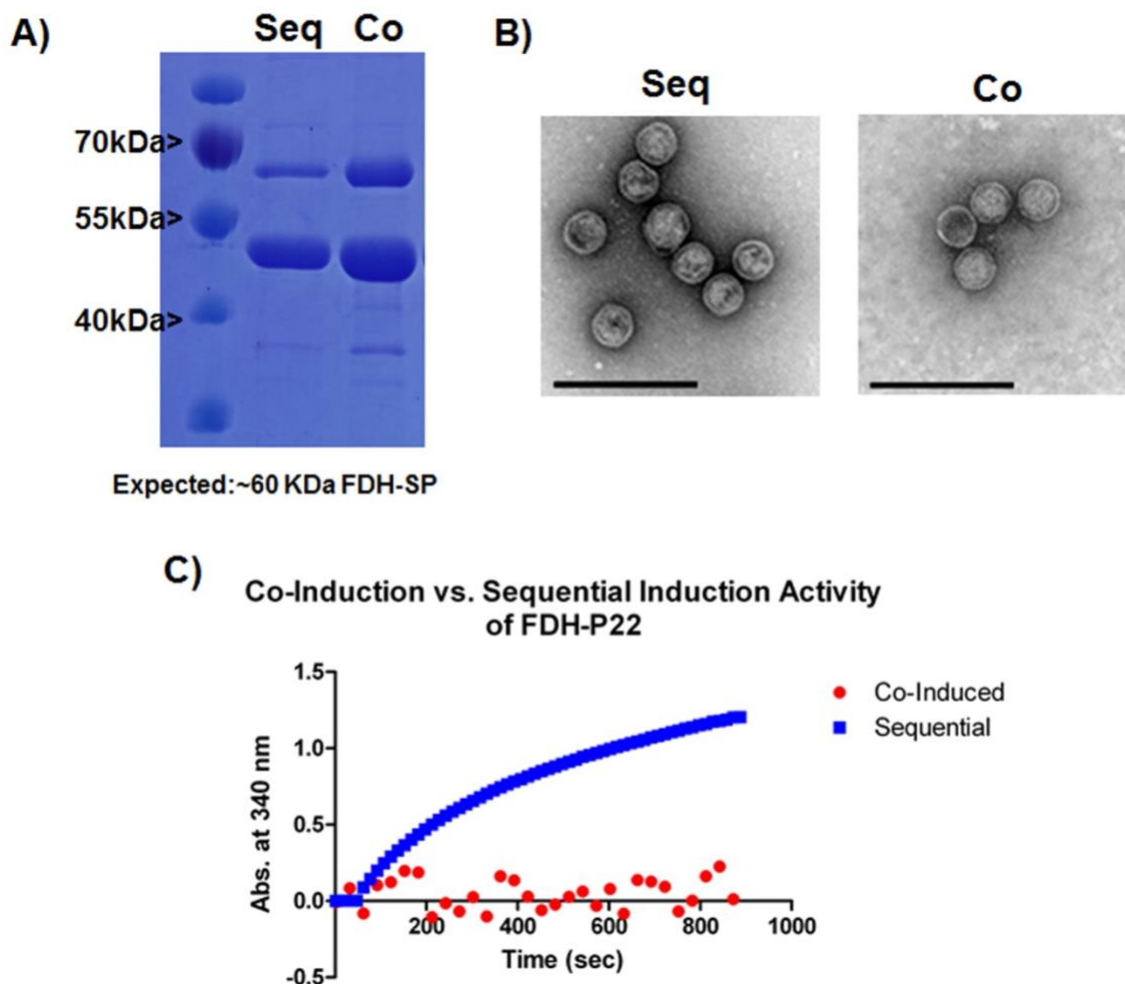


Figure 6. Comparison of FDH-P22 produced from either sequential or co-expressed strategies. (A) SDS-PAGE gel results of FDH-P22 produced via sequential (Seq) or co-expression (Co) methods. Both strategies showed co-purification of FDH-SP (59 kDa) and CP (47 kDa) by SDS-PAGE. (B) Transmission electron microscope images showing that both strategies produce P22 nanoparticles that are indistinguishable from one another. Scale bars are 200nm. (C) Comparison of the activity of conversion of formate to carbon dioxide simultaneously converting NAD^+ to $NADH$, by FDH-P22 generated by either sequential or co-expression methods which was monitored at 340 nm. No activity is observed for even high amounts of coFDH-P22, which only shows scattering effects due to the P22 VLP, whereas seqFDH-P22 was found to be highly active. According to Patterson et al.

from the production of CP. The strategy is outlined in **Figure 7**, which compares the different expression strategies for FDH-SP. For the 2 vector approach, the gene encoding FDH was amplified from genomic *C. boidinii* then inserted into pBad, which provides ampicillin resistance

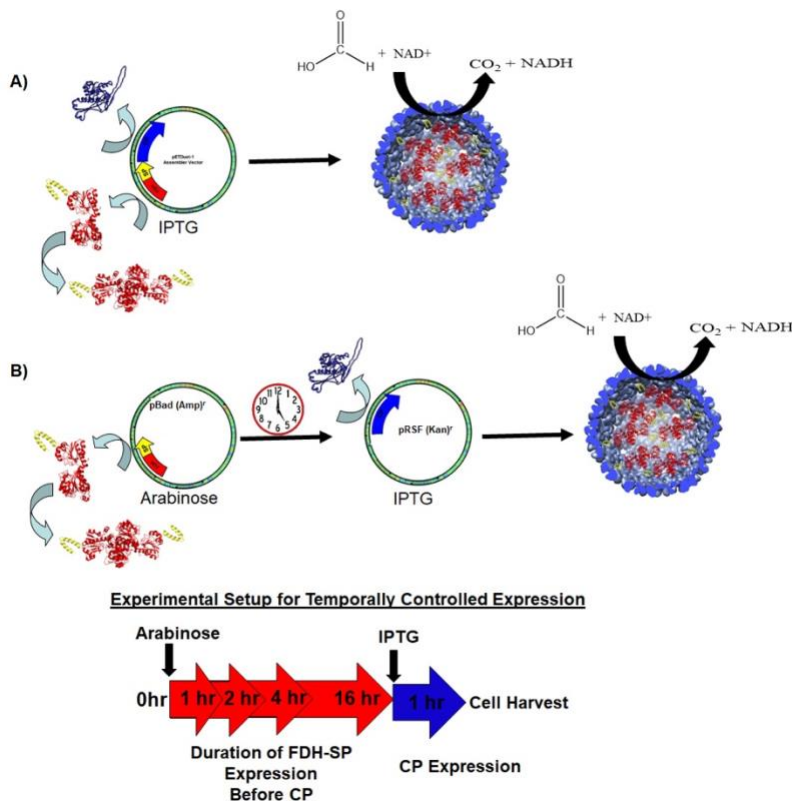


Figure 7. Strategies for encapsulation of active formate dehydrogenase enzyme (FDH).

(A) Single vector approach where Scaffolding protein (SP) is fused with FDH and co-expressed with the bacteriophage P22 VLP coat protein (CP) and inducing expression with IPTG directing encapsulation. (B) Two-vector approach that delays the CP from being expressed by first inducing FDH-SP fused protein with arabinos, allowing time to mature, and then induced the expression of the CP with IPTG to induce encapsulation.

for selection purposes and can be induced by arabinose. The genes encoding CP were inserted into a pRSFDuet-1 vector, which contains kanamycin resistance and is induced by IPTG. The pBad plasmid is only inducible by arabinose, while the pRSFDuet-1 is only inducible by IPTG, allowing temporal control of expression in the different plasmids. It is important to mention that IPTG also suppresses the expression of the pBad plasmid, so once IPTG is added gene expression of the FDH-SP or other enzyme-SP produced using the system is inhibited, largely

preventing or reducing new unmaturing enzymes from being produced once IPTG is added. This system provides an ideal set up for investigating the contribution maturation of enzymes is playing on changes to enzyme kinetics vs. crowding and confinement effects.

Initial enzyme studies of FDH-SP encapsulation were carried out by Dr. Patterson and coworkers, who produced preliminary data for FDH-P22 produced with 2, 4, and 16 hour expression times of FDH-SP before induction of CP and subsequent production of what were termed sequential FDH-P22 VLPs (seqFDH-P22). Summaries of results from these studies are provided in Chapter V to compare with the results that I obtained for times of 0 and 1 hour inductions of FDH-SP before induction of CP. In addition, a secondary enzyme that has been previously studied using the co-expression system, namely AdhD from *Pyrococcus furiosus*, was examined as well to see if changes in catalytic parameters were actually due to crowding and confinement, as previously thought, or were due to maturation effects. AdhD is a monomeric thermostable and hyperthermophile protein which catalyzes the reduction of acetoin (2-hydroxy-2-butanone) to 2,3 butanediol. AdhD contains a high intrinsic resistance to denaturation, leading to prolonged and stable activity. Again, investigations of 2, 4, and 16 hour expression of AdhD-SP before induction of CP were previously determined by others in the Patterson Group, with my contribution focused on ascertaining the effects of early 0 and 1 hour expression times on AdhD-SP activity. Through the use of the two-plasmid system for temporal controlled expression, both FDH-SP and AdhD-SP encapsulation were examined, and new insights were garnered into the role that enzyme maturation plays on the activity of enzymes encapsulated inside the P22 VLP.

IV. MATERIALS AND METHODS

The investigation of the temporally controlled expression of FDH-SP and AdhD-SP in relation to the P22 CP are outlined in the various subsections below.

Materials. DNA modifying enzymes were purchased from New England Biolabs (Ipswich, MA) and Promega (Madison, WI). The pBAD plasmid was purchased from Life Technologies (Grand Island, NY). DNA primers were purchased from Eurofins MWG Operon (Huntsville, AL). *E. coli* BL21(DE3) chemically competent and 10G electrocompetent cells were purchased from Lucigen (Middleton, WI). *Candida boidinii* cell stock was purchased from ATCC (Manassas, VA). QIAquick gel extraction kit and QIAprep Spin Miniprep kit were purchased from Qiagen (Valencia, CA). All chemical reagents were from Fisher Scientific (Pittsburgh, PA) or P212121, LLC (Ypsilanti, MI).

Molecular Biology. The gene encoding FDH was amplified from genomic DNA extracted from *Candida boidinii* using the primers 5'-AAAAAAGCTTCCATGGCAAA GATTGTCTTAGTTCTTTATGATGCTGGTAAGCAC-3' and 5'-AAAAGAGCTCGG ATCCTTTCTTATCGTGTTTACCGTAAGCTTTAGT-3', containing NcoI and BamHI restriction enzyme sites, respectively, which were utilized for insertion of the FDH gene into the pETDuet Assembler Vector containing P22 SP and CP, according to the procedure previously described. The genes encoding FDH-SP and AdhD-SP were removed from the pETDuet Assembler vector by digestion with NcoI and SacI restriction enzymes and transferred to a pBAD vector treated with the same restriction enzymes and ligated with T4 DNA ligase. Ligation reactions were transformed into *E. coli* 10G electrocompetent cells

and plated on LB agar plates containing ampicillin for selection. Colonies resulting from transformation of the ligation were screened by colony PCR and all hits were sequenced (Eurofins MWG Operon) for complete verification. After verifying the correct sequences, DNA was transformed into BL21(DE3) for expression. For sequential expression, pBAD vector (ampicillin resistance) containing the Enzyme-SP protein fusion gene (FDH-SP or AdhD-SP) was co-transformed with a pRSF vector (kanamycin resistance) containing P22 CP, and media containing both ampicillin and kanamycin was used to provide selection for bacteria containing both plasmids. For FDH-SP controls the single pBAD vector was transformed and the media supplemented with ampicillin for selection.

Heterologous Expression and Purification. Co-expression of FDH-SP and CP via the pET-Duet Assembler Vector was carried out as previously described for other P22 constructs. *E. coli* BL21(DE3) strains (Lucigen) harboring constructs for sequential expression (i.e., containing both pBAD and pRSF vectors) were grown in LB medium at 37 °C in the presence of ampicillin (0.1 mg/ml) and kanamycin (0.05 mg/ml) to maintain selection for the plasmids. Expression of the enzyme-SP fusion protein was induced by addition of L-arabinose to a final concentration of 33.3 mM once the cells reached mid log phase ($OD_{600}=0.8$) and cultures were grown for 2-16 hours, after which isopropyl β -D-thiogalactopyranoside (IPTG) was added, to a total concentration of 0.5 mM, to induce expression of CP. Subsequently, cells were harvested by centrifugation after allowing 1 hour induction with IPTG and cell pellets were stored at -20 °C overnight. Co-expression of the dual vector system, to produce 0 hour constructs, was performed by addition of both IPTG and arabinose at the levels used for sequential expression and expression was allowed to go

overnight before harvesting by centrifugation. Purification was carried out as previously described. Briefly, cell pellets were resuspended and lysed by sonication and insoluble cell matter removed by centrifugation at 12,000 x g for 45 minutes. Ultracentrifugation over a 35% (w/v) sucrose cushion on a Sorvall wX+ Ultra Series centrifuge (Thermoscientific) at 38,000 rpm using a Fiberlite F50L-8x39 rotor yielded highly pure viral pellets, which were subsequently resuspended in PBS and further purified by size exclusion chromatography and/or ultracentrifugation over a cesium chloride gradient (0.2 mg/ml to 0.4 mg/mL in PBS) at 38,000 rpm on a Sorvall wX+ Ultra Series centrifuge (Thermoscientific) using a TH-641 rotor. VLPs were concentrated and transferred into PBS by ultracentrifugation and VLP pellets resuspended in PBS with rocking at 4°C.

Free FDH-SP was produced using the pBAD vector containing FDH-SP transformed into BL21(DE3). Cells were grown in LB media supplemented with ampicillin (0.1 mg/mL) and induction carried out by addition of 33.3 mM L-arabinose once the cells reached mid log phase ($OD_{600}=0.8$), and cultures were incubated for 16 hours. Controls examining expression of FDH-SP from pBAD in the presence of the empty pRSF-Duet plasmid were produced in the same way as for free FDH-SP, but with addition of kanamycin for selection and IPTG (0.5 mM) during induction. Cells were harvested by centrifugation and subsequently resuspended in buffer as previously described for FDH. Subsequently, the cell suspension was sonicated using a Qsonica sonicator and centrifuged on a Beckman Alegra benchtop centrifuge at 12,000 x g for 45 min at 4 °C to remove cell debris. The FDH-SP protein was purified by performing Ion Exchange Chromatography of the sonicate supernatant using a MonoQ anion exchange resin on a Biorad NGC FPLC via a linear gradient elution of a 10

mM sodium phosphate, 10 mM sodium chloride, pH 7.4 buffer and 10 mM sodium phosphate, 1 M sodium chloride, pH 7.4 buffer. Samples containing FDH-SP were subsequently dialyzed against 100 mM potassium phosphate, pH 7.4 and stored at 4 °C until performing analyses (Patterson, D. P et al. 2012).

All FDH samples were handled in a way to minimize exposure to light as much as possible under the conditions present in our lab to prevent light inactivation of the enzyme. Samples were covered with aluminum foil after purification and placement into microcentrifuge tubes. In addition, it was found that consistent results for FDH activity required growth and expression from colonies taken from recently transformed plates and not from long term storage glycerol stocks of frozen cell culture maintained at -80 degrees C.

SDS-PAGE. Protein samples were mixed with 4X loading buffer containing DTT and heated in a boiling water bath for 10 minutes, and subsequently spun down on a bench top centrifuge. Samples were separated on a gel containing a 5% polyacrylamide stacking gel and a 18% polyacrylamide running/separating gel using a constant current of 35 mA for approximately 1-1.5 hours. Gels were stained with Coomassie blue and destained or stained with InstantBlue (Expedeon) according to the manufacturer's directions. Images were taken on a UVP MultDoc-IT Digital Imaging System or AlphaImager Mini (Protein Simple) and analyzed using the AlphaView SA software.

Densitometry. Densitometry was performed on SDS-PAGE results to determine relative amounts of FDH-SP or AdhD-SP to CP using AlphaView SA software and the Band

Analysis module according to the manufacturer's directions. Relative ratios of enzyme-SP to CP were utilized to determine enzyme concentrations in samples as previously described for use in kinetics analyses (Patterson, D. P et al. 2012).

Size Exclusion Chromatography with Multiangle Light Scattering and Refractive Index Detection. Samples separated over a WTC-0200S (Wyatt Technologies) size exclusion column utilizing an Agilent 1200 HPLC to apply and maintain a 0.7 mL/minute flow rate of 50 mM phosphate, pH 7.2 buffer containing 100 mM sodium chloride and 200 ppm sodium azide. Samples of 25 μ L were injected onto the column and total run time was 30 minutes. Samples were detected using a UV-Vis detector (Agilent), a Wyatt HELEOS Multi Angle Laser Light Scattering (MALS) detector, a quasi-elastic light scattering detector (QELS), and an Optilab rEX differential refractometer (Wyatt Technology Corporation). The number average molecular weight, M_n , was calculated with Astra 5.3.14 software (Wyatt Technology Corporation) based on the molecular weight distribution. Molecular weights determined for empty P22 VLPs was subtracted from molecular weights determined for enzyme loaded P22 VLPs to determine the mass of enzyme encapsulated, which was utilized to calculate the loading of enzymes per VLP by dividing by the molecular weight of the individual enzyme-scaffolding proteins calculated from the amino acid sequence. Enzyme packaging per particle was used to determine relative ratios of enzyme concentrations as previously describe.

Transmission Electron Microscopy. Samples (10 μ L, 0.1 mg/mL protein) were applied to glow discharged formvar coated grids and incubated for 30 seconds and excess liquid was

removed with filter paper. Grids were then washed with 10 μ L of distilled water, liquid was removed with filter paper shortly after addition, and then stained with 5 μ L 2% uranyl acetate after which excess stain was removed with filter paper. Images were taken on a JEOL JEM 1010 transmission electron microscope at accelerating voltage of 100 kV.

Enzyme Kinetics Assays. Activity assays were carried out on a Cary 300 Bio UV-Visible Spectrophotometer fitted with a Cary Dual Cell Peltier Accessory for heating. For FDH assays, buffers were preheated in the hot water bath connected with the temperature control module that maintained constant a temperature of 30 °C on the spectrophotometer cuvette holder. Kinetics assays for FDH were carried out in 100 mM potassium phosphate buffer, pH 7.5, in a similar manner as describe previously. Briefly, buffer solutions containing formate concentrations ranging from 0.5-100 mM were placed in a cuvette with NAD⁺ (300 μ M) and the instrument was blanked. After blanking, FDH sample was added to the activity assay solution, mixed in the cuvette by pipetting, and the production of NADH was monitored at 340 nm for 3-5 minutes. Assays for AdhD-P22 were carried out as previously described using the same instrumentation as the FDH assays with an evaluation at a temperature at 50 °C. To briefly summarize AdhD-P22 activity assays, preheated (50 °C) buffer solutions containing acetoin concentrations ranging from 0.1-100 mM were placed into a heated cuvette and the solution was blanked. A small volume of NADH was added to produce 300 μ M NADH, which was checked in the spectrometer which was check before addition of AdhD to determine the rate of non-enzymatic thermal degradation of NADH. AdhD was added to the cuvette, the solutions were mixed thoroughly by pipetting, and the loss of NADH was monitored at 340 nm for 3-5 minutes. The non-enzymatic thermal

degradation rate of NADH was subtracted from the enzymatic rate of NADH during data processing. Data from kinetics runs for both enzymes were processed in Excel to determine the initial velocities at each substrate concentration, which were converted to turnover by dividing by the total enzyme concentration utilized in the run. Absorbance values from assays were converted to concentration using the extinction coefficient at 340 nm for NADH (ϵ_{340}) of $6,220 \text{ M}^{-1}\text{cm}^{-1}$. Total enzyme concentrations were determined from the ratios of enzyme to CP found by SEC-MALS or SDS-PAGE densitometry according to methodology previously described. Free FDH-SP was calculated directly from its solution absorption at 280 nm and the extinction coefficient for FDH-SP. Extinction coefficients (ϵ_{280}) used in calculating protein concentrations were $55,450 \text{ M}^{-1}\text{cm}^{-1}$ for FDH-SP, $44,380 \text{ M}^{-1}\text{cm}^{-1}$ for CP, and $62,990 \text{ M}^{-1}\text{cm}^{-1}$ for AdhD-SP, which were calculated using Protein Calculator v3.3 or v3.4 (Chris Putnam, The Scripps Research Institute, USA). Data was further analyzed using Prism 5 (GraphPad Software) graphing software by fitting with the Michaelis-Menten non-linear fitting function to determine kinetics parameters. Comparative statistical analysis was performed on kinetics parameters using the student's t-Test in the Excel software package. The turnover per enzyme density was determined individually for each batch, which was compared between time variations by the same Student's t-test analysis as for the kinetics parameters.

V. INVESTIGATIONS AND FINDINGS FOR 0 HOUR AND 1 HOUR ENCAPSULATION STRATEGIES

A. Temporal Investigation of Formate Dehydrogenase

The focus of the investigation was to determine the effects of temporal delays on the folding and then encapsulation of FDH-SP enzymes determined by their catalytic activity. Investigations carried out by me focused on no delay between the induction of FDH-SP and CP, henceforth termed 0 hour delay, and a 1 hour delay between the induction of FDH-SP and the CP using the two-plasmid expression system described previously. After production of the 0 hour and 1 hour seqFDH-P22 VLPs, the VLPs were characterized by SDS-PAGE. Results from the SDS-PAGE showed bands of 59 kDa for the FDH-SP and 47 kDa for the CP (**Figure 8**), consistent with co-purification and likely encapsulation of FDH-SP inside P22 VLPs.

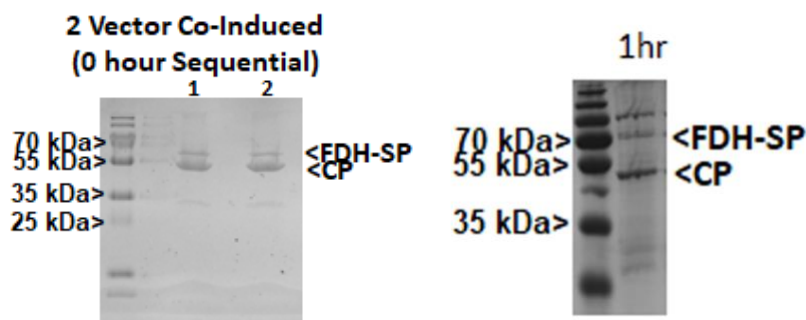


Figure 8. *SDS-PAGE Characterization of FDH-P22 produce by sequential induction by using a two-plasmid system.* The figure represents the SDS-PAGE analysis for the 0 and 1 hour construct. Two batches of the 0 hour construct are being represented by the lanes labeled 1 and 2.

In complement to the SDS-PAGE characterization, TEM images of the 0 hour and 1 hour constructs showed particles with diameters of 62.2 ± 1.9 nm 61.6 ± 2.0 nm, consistent with the expected diameter of 58 nm for the T=7 icosahedral capsid of the expected structures (**Figure 9**).

Overall, TEM showed well-formed particles, although the 0 hour did show some mis-formed aggregates, possible due to limited FDH-SP available during assembly. The particle size and molar mass was also evaluated by size exclusion chromatography coupled to in-line angle light scattering, quasi-elastic light scattering, and refractive detectors (SEC-MALS/QELS/RI),

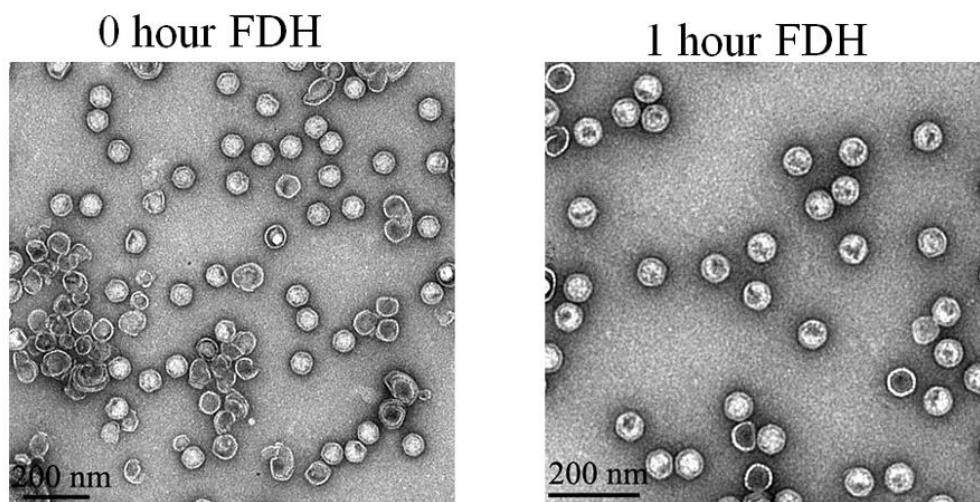


Figure 9. Transmission electron microscope FDH-P22 Characterization. The TEM images of the 0 and 1 hour constructs produced using a two-plasmid approach. The 0 hour construct show abnormal formation of the FDH-P22.

resulting in the 30.7 ± 0.6 MDa for the 0 hour and 30.6 ± 0.6 MDa for 1 hour (**Figure 10**), corresponding to 164 ± 11 and 168 ± 11 copies of FDH-SP encapsulated, respectively, significantly lower than 215 ± 3 copies of FDH-SP encapsulated by the single plasmid co-induction strategy (coFDH-P22). In addition, the 0 hour and 1 hour seqFDH-P22 samples showed lower encapsulation values in comparison to 2, 4, and 16 hour samples of seqFDH-P22 examined previously. Overall, the results indicate that an increase in induction time of FDH-SP before induction of the CP leads to an increased amount of FDH-SP encapsulated, with the 16 hour seqFDH-P22 values nearing the amount observed for coFDH-P22. The SEC-MALS/QELS/RI results also allow us to study the hydrodynamic radius (R_h), representing the outer diameter of the VLP, and the apparent VLP structure being spherical and the radius of gyration (R_g),

representing the mass weighted distance from the core of the molecule. The ratio of R_g to R_h (R_g/R_h) provides an indication of the packing density, with an $R_g/R_h=1$ for hollow spherical particles with infinitely thin shells and R_g/R_h of less than 1 for spherical particles with thicker walls or solid spheres.

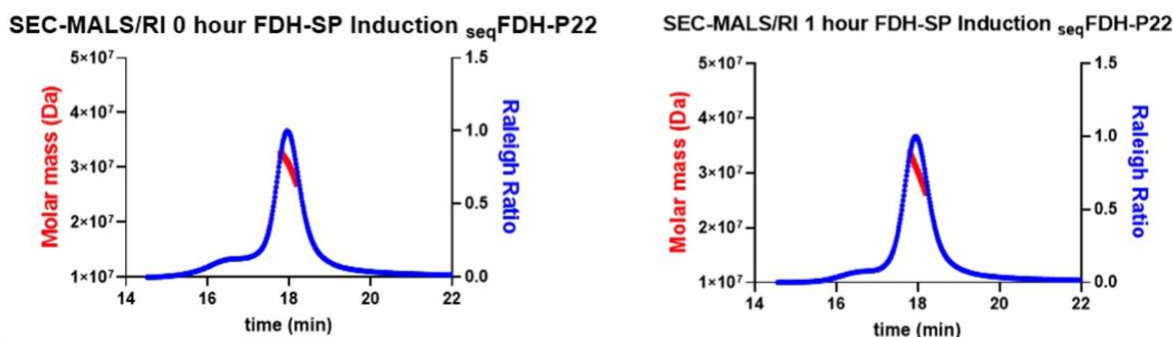


Figure 10. Characterization of FDH P22 construct by SEC-MALS/2ELS/RI. SEC chromatograms for FDH-P22 produce with two plasmid system providing the 0 and 1 hour constructs.

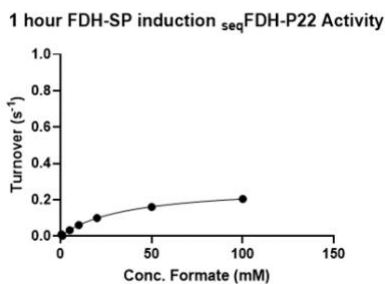
The hydrodynamic radius of the purified P22 VLPs were found to be consistent across the board regardless of the amount of FDH-SP induction time. The SEC-MALS/QELS/RI (**Figure 10**) show us the R_g/R_h ratio to be 0.84 for the 0 hour construct, while the 1 hour construct resulted in a R_g/R_h ratio to be that of 0.87, which presents the tight internal packaging of the VLP with the FDH enzyme. Additionally, we are able to compare the different constructs as it is summarized in **Table 1**. The R_g/R_h values of near 0.90 for all constructs are consistent with dense packaging of FDH-SP on the interior of the P22 capsid. Although TEM images for 0 hour showed some mis-formed particles, likely due to lower FDH-SP available to template assembly, overall SEC-MALS/QELS/RI and TEM show well formed P22 VLPs with sizes and packaging consistent with the formation of intact P22 VLPs encapsulating FDH-SP.

Table 1. Determination of FDH-P22 VLP molar mass, packaging, and solution radii analysis by SEC-MALS/QELS/RI. Increased copies of FDH were observed with increased induction times of FD-SP, maintaining overall packaging of the interior as evidenced by the Rg/Rh. Single vector co-induced FDH-P22 showed the highest packaging, with the longest sequential expression strategy showing comparable packaging levels of FDH. The table shows previous data from 2 to 16 hours before encapsulation, and the 0 to 1 hour of this study.

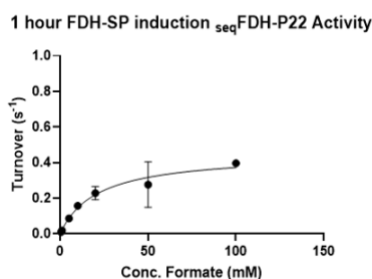
Sample	Molar Mass (MDa)	Copies of FDH	Rh (nm)	Rg (nm)	Rg/Rh
coFDH-P22	32.3 ± 0.3	215 ± 3	26.4 ± 0.3	22.8 ± 0.2	0.86
0 hr seqFDH-P22	30.7 ± 0.6	164 ± 11	27.3 ± 0.7	23.0 ± 0.1	0.84
1 hr seqFDH-P22	30.6 ± 0.6	168 ± 11	26.2 ± 0.5	22.8 ± 0.2	0.87
2 hr seqFDH-P22	28.2 ± 0.5	145 ± 8	26.5 ± 0.1	23.9 ± 0.1	0.90
4 hr seqFDH-P22	30.3 ± 0.2	181 ± 3	26.1 ± 0.3	23.4 ± 0.1	0.90
16 hr seqFDH-P22	31.8 ± 0.1	206 ± 2	26.0 ± 0.0	23.3 ± 0.1	0.90

To further characterize the FDH-P22 activity, the oxidation of formate through the reduction of NAD⁺ was measured through UV-Vis at 340 nm. Interestingly, the 0 hour seqFDH-P22 showed nearly non-existent activity, with a turnover of 0.006 s⁻¹ observed for one prep and none for the others. This result was consistent with the coFDH-P22, which was produced by co-expression on a single plasmid. However, when the 1 hour seqFDH-P22 was examined, it showed activity for all three preparations analyzed (**Figure 11**), with average kinetics parameters 0.39±0.08 s⁻¹ for k_{cat}, 32.4±8.15 for K_M, and 0.013±0.006 for k_{cat}/K_M mM⁻¹s⁻¹.

Trial 1



Trial 2



Trial 3

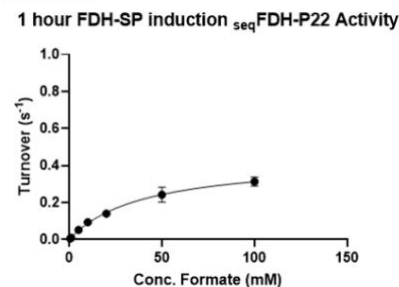


Figure 11. Evaluation of FDH-P22 kinetics with variation of formate concentration. Plots showing the results of kinetics assays from FDH-P22 produced with 1 hour delay. Data is fit to a Michaelis-Menten equation.

Additionally, the Patterson group generated data for 2, 4 and 16 hour temporal delay, along with a non-encapsulated FDH-SP (free FDH-SP) control, which is displayed in **Table 2**.

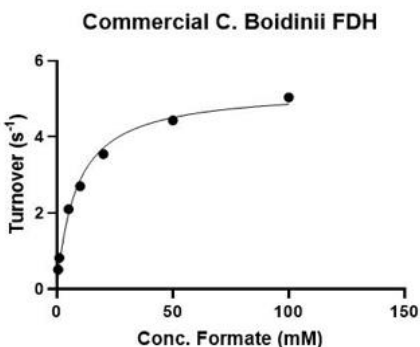


Figure 12. *Evaluation of Candida Boidinii FDH control kinetics analyzed through a variation of formate concentrations. The plot was produced through the analysis of industrially produced FDH and purchased from Sigma Aldrich.*

Results from the kinetic assays showed a general trend of increased k_{cat} values for more extended FDH-SP induction, although some variability was observed from batch to batch. In comparison to the free FDH-SP, all seqFDH-P22 samples showed higher k_{cat} values, with only the 16 hour seqFDH-P22 being statistically relevant. The K_M values were found to be similar only between the free FDH-SP and 1 hour seqFDH-P22, which showed a much higher and statistically significant K_M from its seqFDH-P22 counterparts. Taken together the results suggest that shorter induction times before encapsulation leads to kinetics values more similar to free FDH-SP, with longer FDH-SP induction before encapsulation leading to lower K_M and higher k_{cat} kinetic parameters, resulting in greater catalytic efficiency as observed in **Table 2**.

Table 2. The results show the average apparent kinetic parameters. Three independent preparations for FDH-P22 produced via co-expression, sequential expression (0 hr, 1 hr, 2 hr, 4 hr, and 16 hr) and encapsulation strategies, as well as non-encapsulated FDH

Sample	k_{cat} (s^{-1})	$K_{M,app}$ Formate (mM)	k_{cat}/K_M ($mM^{-1}s^{-1}$)
coFDH-P22	No Activity	No Activity	No Activity
0 hr seqFDH-P22	No Activity	No Activity	No Activity
1 hr seqFDH-P22	0.39 ± 0.08	$32.4 \pm 8.1^{\$}$	0.013 ± 0.008
2 hr seqFDH-P22	0.48 ± 0.03	13.8 ± 2.9	0.034 ± 0.011
4 hr seqFDH-P22	0.70 ± 0.47	9.4 ± 1.7	0.070 ± 0.043
16 hr seqFDH-P22	$0.70 \pm 0.18^*$	13.7 ± 0.9	0.052 ± 0.017
free FDH-SP	$0.33 \pm 0.04^*$	23.2 ± 5.1	0.014 ± 0.001

A closer evaluation of the kinetics parameters of FDH-P22 and FDH-SP in comparison to those published in the literature for FDH found that the kinetics parameters in our experiments were comparable for K_M but show significant differences in k_{cat} . In the literature K_M values of 4-20 mM for formate were found, with the 1 hour seqFDH-P22 even being close to the high K_M range values published considering the standard deviation. However, k_{cat} values of nearly tenfold or more lower are found for FDH-SP and seqFDH-P22, with turnovers of 2-6 s^{-1} found by others, depending on the study, which was surprising. Differences in the observed k_{cat} values could be due to differences in our preparation methods and handling compared to those performed by others or due to genetic attachment of SP to FDH to produce FDH-SP. To examine the difference in k_{cat} further, I performed kinetic assays on authentic *C. boidinii* FDH (**Figure 12**) that was purchased from a commercial source. Commercial *C. boidinii* FDH showed kinetic parameters of 5.26 s^{-1} for k_{cat} and 8.4 mM for K_M (**Table 2**), consistent with published values, suggesting that fusion of SP to FDH may alter the kinetics.

An additional FDH-SP control was produced by expression of FDH-SP from pBAD in the presence of an empty pRSFDuet-1 vector (co-induced with IPTG) to see if the presence of the pRSFDuet-1 showed any effect on the kinetics of FDH-SP and the differences seen for the seqFDH-P22 samples. The FDH-SP produced in the presence of empty pRSFDuet-1 plasmid yielded an average k_{cat} of $0.21 \pm 0.03 \text{ s}^{-1}$ and K_M of $9.7 \pm 1.1 \text{ mM}$ (**Figure 13**), showing values that are lower in both k_{cat} and K_M than free FDH-SP and most of the encapsulated seqFDH-P22 samples. For K_M , the value was found to be statistically lower for FDH-SP produced in the presence of pRSFDuet-1 than the free FDH-SP control, 1 hour seqFDH-P22, and 16 hour seqFDH-P22 (p values of 0.0234, 0.0173, and 0.0084, respectively). The k_{cat} FDH-SP produced in the presence of empty pRSFDuet-1 plasmid was found to be statistically lower than all but the 4 hour seqFDH-P22, with p values ranging from 0.0041 to 0.0359 for the statistical analysis. Taken together the results from the FDH-SP control produced in the presence of an empty pRSFDuet-1 vector during expression shows a possible negative effect on k_{cat} , in contrast to the improved k_{cat} values found for seqFDH-P22 samples that were also produced with pRSFDuet-1 present. No consistent finding is observed for the K_M , since free FDH-SP control produced without pRSFDuet-1 present and the 1 hour seqFDH-P22, which was produced with the pRSFDuet-1 plasmid present, both had higher K_M values, suggesting that the pRSFDuet-1 was not influencing the K_M values observed. While a free FDH was not produced, the comparative studies performed between FDH-SP ensure that the kinetic differences observed for encapsulation were not due to preparation and handling or variations between the enzymes being encapsulated and serve the desired purpose of the study.

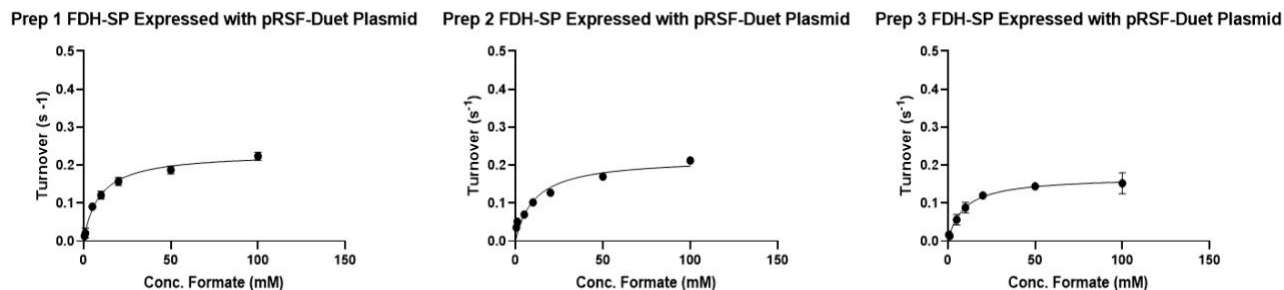


Figure 13. *Evaluation of Kinetics of FDH-SP produced in the presence of an empty pRSFDuet plasmid*

Overall, the activity of the encapsulated of the FDH improved when there was an increased time delay between the induction of the FDH-SP and the CP. The findings also suggests that the crowding and confinement may play a role in the activity of the encapsulated FDH enzyme, as we see an increase in activity with increased enzyme packaging load, which in general increases with increased delay time before induction of CP as displayed in **Figure 14**.

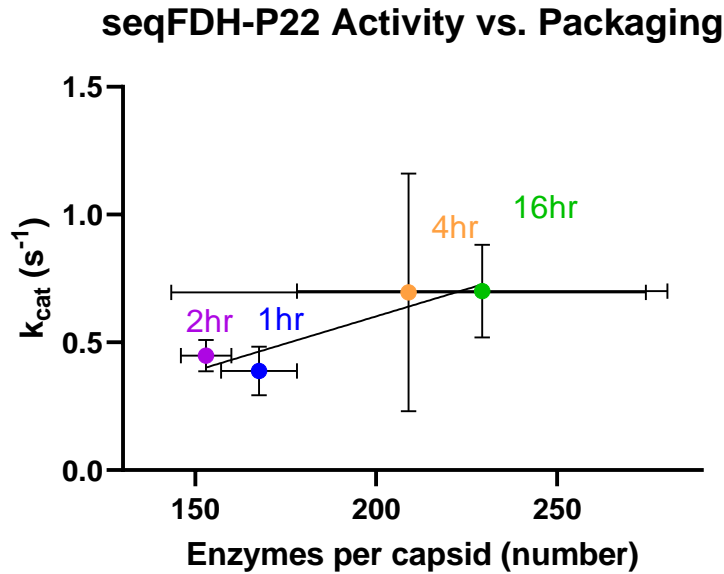


Figure 14. Comparison of FDH activity per enzyme encapsulated inside the P22 VLP by sequential induction. Enzyme activity per enzyme encapsulated showed no significant change between induction times of FDH-SP. The enzyme activity per enzyme encapsulated were by dividing the average K_{cat} by the average number of enzymes encapsulated for 3 batches produced. Error bars indicate the standard deviation found for each data set.

B. Temporal investigation of Alcohol Dehydrogenase D

In the past, Patterson et al. were able to produce an active AdhD-P22 VLP through a single plasmid methodology, obtaining a k_{cat} of $0.097 \pm 0.005 s^{-1}$ presenting that the enzyme had enough time to fold and mature in order to be active. They also obtained a K_M of 1.23 ± 0.21 mM, and a k_{cat}/K_M of $0.079 mM^{-1}s^{-1}$ while free AdhD-SP showed to have a k_{cat} of $0.77 \pm 0.03 s^{-1}$, K_M of 6.23 ± 0.21 mM, with a catalytic efficiency (k_{cat}/K_M) of $0.124 mM^{-1}s^{-1}$ (Patterson et al. 2012). Recently, others have examined an *in vitro* encapsulation method to produce AdhD-P22 that showed slightly altered results with k_{cat} of $0.46 \pm 0.02 s^{-1}$, K_M of 4.67 ± 0.30 mM, with a catalytic

efficiency (k_{cat}/K_M) of $0.1 \pm 0.01 \text{ mM}^{-1}\text{s}^{-1}$. It can be observed that the co-induced construct has lower values than the *in vitro* constructs reported by Sharma et al, and substantially lower than the free AdhD-SP construct. It was hypothesized that the two-plasmid system could be used to improve the activity of the encapsulated AdhD *in vivo*. To examine the hypothesis, the genes that encode AdhD-SP were put into the pBAD plasmid (ampicillin resistant and induce by arabinose), while the genes encoding for the CP was cloned into the pRSFDuet-1 plasmid (kanamycin resistant and induced by IPTG). Again, using this methodology with two different antibiotic resistances allows for the selection of *E.coli* colonies that contain both plasmids, ensuring the ability to express both AdhD-SP and CP within the same cell.

The two-plasmid system expression, purification, and characterization of AdhD-P22 VLPs was carried out in the same fashion as seqFDH-P22, including characterized by SDS-PAGE, SEC-MALS/QELS/RI, and TEM. Again, the focus of the studies that I carried out were on 0 hour and 1 hour time delays after induction of AdhD-SP before CP was induced. Results produced the expected bands of 50 kDa for the AdhD-SP, and 47 kDa for the CP (**Figure 15**).

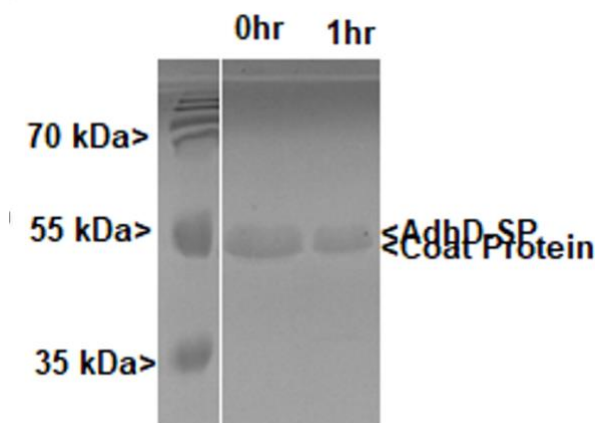


Figure 15. SDS-PAGE Characterization of AdhD P22. The 0 and 1 hour samples showed poor separation, which has been seen for AdhD-SP and CP in previous studies. SEC-MAL/RI helped further confirmation of AdhD-SP was encapsulated in the P22 VLP.

The TEM analysis of the purified particles showed formation of regular P22 VLPs with average diameters of 60.4 ± 3.9 , and 62.0 ± 2.7 nm for 0 and 1 hours (**Figure 16**), respectively, comparable to 54.4 ± 1.9 observed previously for the coAdhD-P22. It can be observed that the 0 hour sample of the seqAdhD-P22 produced some aberrant assemblies, similar to the previous results found for 0 hour seqFDH-P22, supporting the hypothesis that lower enzyme-SP levels leads to more aggregate and mis-formed P22 VLPs.

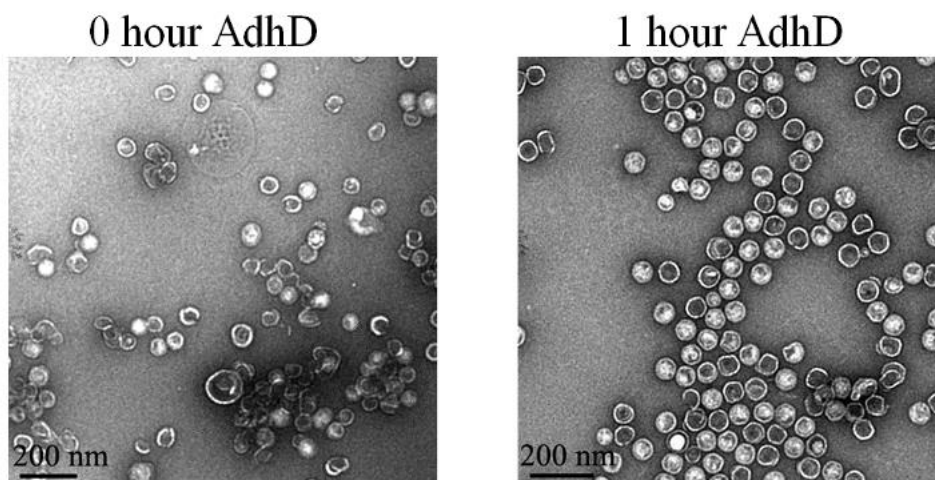


Figure 16. Characterization of seqAdhD-P22 by transmission electron microscopy. TEM images of seqAdhD-P22 produced with 0 and 1 hour delays. TEM samples are compared to previous studies performed by the Patterson research group.

Additional support for lower expression of enzyme-SP for loading comes from SEC-MALS/QEL/RI, where a lower loading of the AdhD-SP was found for the 0 hour and 1 hour constructs compared with previous data gathered by the Patterson group, as shown in **Table 3**. Overall, the particles produced similar Rg/Rh ratio range from 0.81 to 0.92, indicating spherical particles with dense packing. Interestingly, lower levels of AdhD-SP enzyme were found to be encapsulated relative to the FDH-P22 VLP.

The Rg/Rh values of near 0.90 for all constructs are consistent with dense packaging of AdhD-SP on the interior of the P22 capsid. Although TEM images for 0 hour showed some mis-formed particles, likely due to lower AdhD -SP available to template assembly, overall SEC-MALS/QELS/RI and TEM show well formed P22 VLPs with sizes and packaging consistent with the formation of intact P22 VLPs encapsulating AdhD-SP.

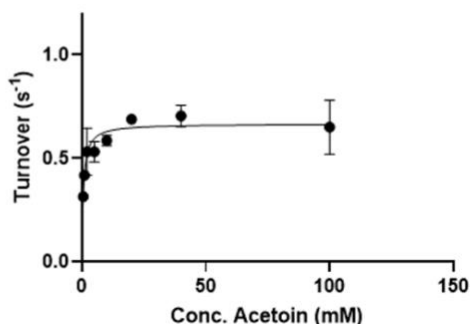
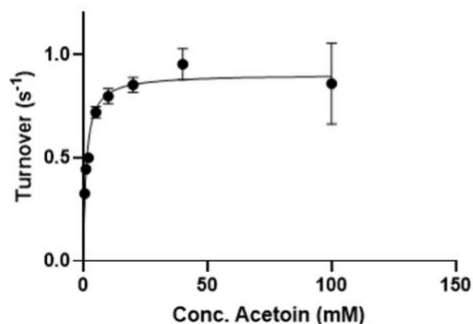
Table 3. Determination of AdhD-P22 VLP molar mass, packaging, and solution radii analysis by SEC-MALS/QELS/RI. Increased copies of AdhD were observed with increased induction times of AdhD-SP.

Sample	Molar Mass (MDa)	Copies of AdhD	Rh (nm)	Rg (nm)	Rg/Rh
0 hr seqAdhD-P22	27.6 ± 2.6	138 ± 51	30.2±0.2	24.6±0.6	0.81
1 hr seqAdhD-P22	29.0 ± 1.5	165 ± 10	27.7±0.9	23.4±0.6	0.84
2 hr seqAdhD-P22	28.2 ± 0.13	169 ± 3	25.9±0.1	23.7±0.0	0.92
4 hr seqAdhD-P22	28.4 ± 0.49	172 ± 10	26.5±0.1	23.8±0.0	0.90
16 hr seqAdhD-P22	31.0 ± 0.47	224 ± 9	26.3±0.1	23.3±0.1	0.89

Kinetic assays were performed in order to analyze the catalytic activity of the encapsulated AdhD, obtained in triplicate for each construct trial, with a variation of acetoin concentrations used in the kinetic assays to analyze the oxidation of NADH to NAD⁺, at a constant temperature of 50 °C (**Figure 17**). Turnover rates were not significantly different for the 0 hour and 1 hour seqAdhD-P22 vs. values previously found, with k_{cat} values ranging from 0.55-0.96 sec⁻¹. The two vector expression data tracks more closely to the k_{cat} value of 0.77 sec⁻¹ observed previously for free AdhD-SP compared with the previous observation of only 0.1 sec⁻¹ for the coAdhD-P22 constructs previously examined by the author (**Table 4**).

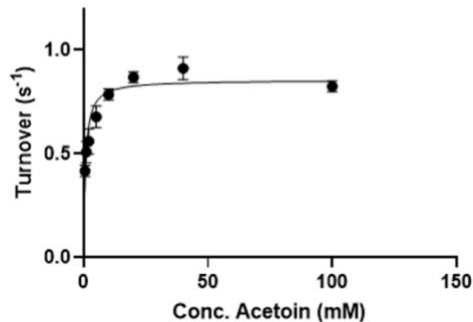
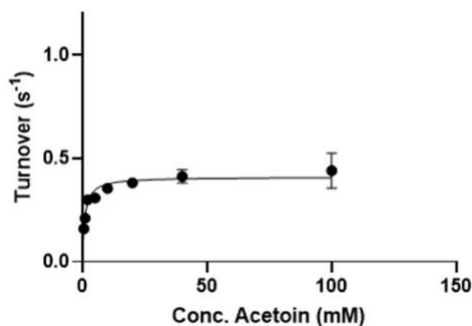
Trial 1

0 hour AdhD-SP induction $_{seq}$ AdhD-SP Activity 1 hour AdhD-SP induction $_{seq}$ AdhD-SP Activity



Trial 2

0 hour AdhD-SP induction $_{seq}$ AdhD-SP Activity 1 hour AdhD-SP induction $_{seq}$ AdhD-SP Activity



Trial 3

0 hour AdhD-SP induction $_{seq}$ AdhD-SP Activity

1 hour AdhD-SP induction $_{seq}$ AdhD-SP Activity

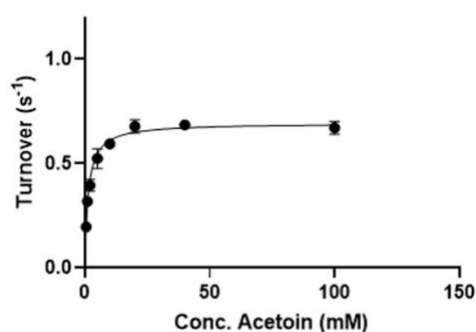
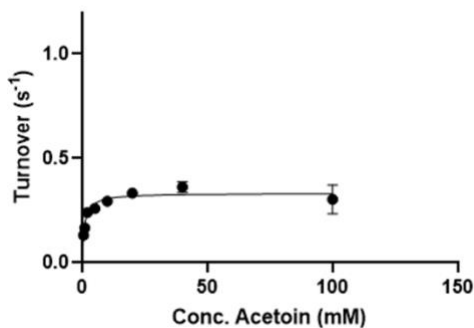


Figure 17. Evaluation of AdhD-P22 kinetics with variations of Acetoin concentrations. Plots showing the kinetics assays for AdhD-P22 produced with 0, and 1 delay between AdhD-SP and CP induction.

Table 4. Kinetic parameters determined for AdhD-P22 constructs. The results show the apparent kinetic parameters for AdhD-P22 produced via sequential expression and a comparison with past values obtained from the co-expression strategies, in vivo encapsulation, and the non-encapsulated AdhD-SP (free AdhD-SP) values with *indicate statistical difference (Student t-test $p < 0.05$) vs 2, 4, and 16 hour seqAdhD-P22 samples.

Sample	k_{cat} (s^{-1})	$K_{M,app}$ Acetoin (mM)	k_{cat}/K_M ($mM^{-1}s^{-1}$)
coAdhD-P22 [#]	0.097 ± 0.005	1.23 ± 0.31	0.079
seqAdhD-P22 0 hr	0.55 ± 0.31	$0.99 \pm 0.15^*$	0.55 ± 0.21
seqAdhD-P22 1 hr	0.74 ± 0.10	$0.89 \pm 0.40^*$	0.94 ± 0.37
seqAdhD-P22 2 hr	0.67 ± 0.19	9.4 ± 3.6	0.07 ± 0.02
seqAdhD-P22 4 hr	0.88 ± 0.22	7.9 ± 3.0	0.12 ± 0.06
seqAdhD-P22 16 hr	0.96 ± 0.24	8.3 ± 4.0	0.12 ± 0.03
<i>in vitro</i> AdhD-P22 [#]	0.46 ± 0.02	4.67 ± 0.30	0.1 ± 0.01
free AdhD-SP [#]	0.77 ± 0.03	6.23 ± 0.87	0.124

These results show that 0 hour also had improved activity, with no statistical difference from the other constructs, suggesting that decoupling the expression of AdhD-SP and CP, by placing them on separate plasmids, improves the overall turnover of the enzyme. However, while the K_M values of seqAdhD-P22 constructs produced at 2, 4, and 16 hour AdhD-SP expression were found to be consistent with free AdhD-SP (7.9-8.3 mM vs. 6.23 mM), the 0 hour and 1 hour seqAdhD-P22 constructs showed much lower K_M values that mirrored those found previously for coAdhD-P22 (0.89 and 0.99 mM vs. 1.23 mM). It is unclear why the short expression times, 0 hour and 1 hour, for AdhD-SP before encapsulation changes K_M so drastically. The increased k_{cat} and decreased K_M observed for the 0 hour and 1 hour actually led to an improved catalytic efficiency, k_{cat}/K_M , that is improved over values seen for all other samples. These results suggest that increased induction times are not always necessary for optimal activity and that obtaining improved kinetic efficiency may vary and need to be determined on an enzyme-by-enzyme basis.

seqAdhD-P22 Activity vs. Enzyme Loading

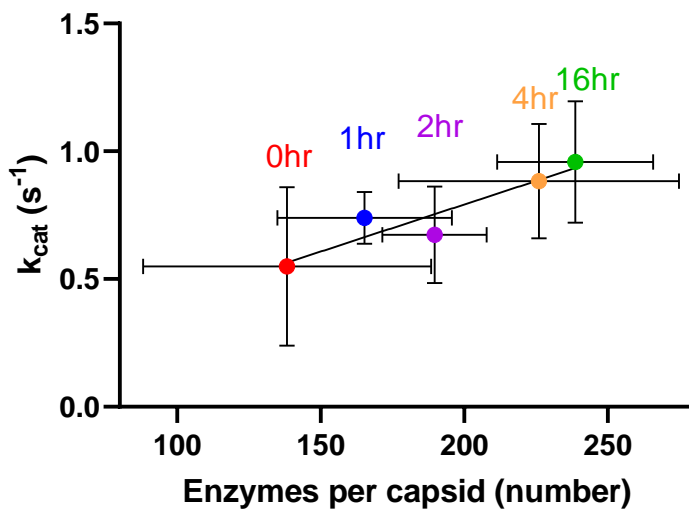


Figure 18. Comparison of AdhD activity per enzyme encapsulated inside the P22 VLP by sequential induction. Enzyme activity per enzyme encapsulated, found by dividing the average K_{cat} by the average number of enzymes encapsulated in a total of three batches produce, was not observed to change significantly between induction times of AdhD-SP.

Further analysis was performed to see if the loading had any effect on activity of seqAdhD-P22 VLPs, by plotting the k_{cat} vs. the number of enzymes encapsulated per VLP, which is shown in **Figure 18**. A linear increase, correlating with an increase in induction time of AdhD-SP before encapsulation, is observed for seqAdhD-P22. Therefore, the findings here do not rule out effects from crowding and confinement, since in all cases the seqAdhD-P22 constructs still showed alleviation of substrate inhibition even though AdhD is well known to have substrate inhibition above concentrations of 40 mM acetoin,¹⁷ well below the substrate levels examined for seqAdhD-P22 constructs here. In addition, an increase in k_{cat} per enzyme is observed for more densely packed seqAdhD-P22, suggesting the improvement may be a result of crowding. These findings suggest that confinement and crowding have the potential to alter the properties, such as enzyme substrate inhibition, and further investigations using encapsulation in VLPs may be used to examine this phenomenon furthermore.

VI. CONCLUSION AND FUTURE DIRECTIONS

This research shows that the methodology employed previously for the encapsulation of enzymes inside of VLPs can have an effect on the activity of the enzymes of interest. Support for this is found from the encapsulation of formate dehydrogenase (FDH) described here, which was found to be inactive when encapsulated in a co-expression of the FDH-SP and CP through either a single or two plasmid approach. However, allowing the FDH-SP to be expressed temporally earlier from CP permitted the maturation of the FDH-SP and activity upon encapsulation. This can additionally be supported by the results for AdhD-SP, which showed a decoupling effect when using the two plasmid system, slightly different from FDH-SP. Moreover, AdhD retained previous kinetic advantages observed upon encapsulation, such as substrate inhibition, using the sequential encapsulation of AdhD-SP.

The results, jointly, presents the improvement of encapsulated enzyme kinetics can be obtained by permitting enzymes to mature before being encapsulated. Additionally, this lays the groundwork for further studies in compartmentalization of enzymes of interest, especially studies involving *in vivo* production and encapsulation, which can be applied in a two-plasmid system to separate the induction and production of the desired enzymes. However, it does demonstrate that the encapsulation system is not a universal application, but rather a unique approach that can be tailored for future enzymes of interest. As showed by the FDH encapsulation, which led to higher K_M values as it had less time to mature before encapsulation, while AdhD-SP K_M values were lower for those constructs with lower induction times. Typically, the longer induction times for the enzyme expression before encapsulation can result in an increase of enzyme maturity, as well as an increase in the number of enzymes being encapsulated inside the VLPs.

VLPs provide unique structures that are both elegant and a solution to packaging, protecting, and transporting molecular cargo. They present a range of structures and can generate a library of protein cages that can be used and applied to different needs. It is important not to see viral structures as merely disease harboring structures that are working against humanity, but to consider them a system that can be modified to become new allies that can be harnessed and utilized for new applications that serve humanity. Future investigations in enzyme encapsulation should look toward single enzyme reactions and identify effects caused by isolation, in addition to examining multiple enzymes encapsulation that can reflect biological pathways. Toward these studies the two plasmid system time delay, permitting the appropriate time for each enzyme to fold and achieve an efficient concentration, may be useful and helpful in advancing the field. In therapeutics, this can permit the encapsulation of enzymes that can be used therapeutically relevant and require temporal expression delays to gain useful activity. Other ways in which this encapsulation strategy may be useful is in the study of stability and folding stages of proteins such as glucose oxidase, lactase, and malate dehydrogenase. This research establishes the groundwork to construct enzyme nanoreactors built on protein cage structures allowing encapsulation of more challenging enzymes that require special maturation before encapsulation.

BIBLIOGRAPHY

1. Agirrezabala, X., Samatova, E., Macher, M., Liutkute, M., Maiti, M., Gil-Carton, D., Novacek, J., et al. (2022). A switch from α -helical to β -strand conformation during co-translational protein folding. *The EMBO Journal*, 41(4), e109175.
2. Aime, S., Frullano, L., & Geninatti Crich, S. (2002). Compartmentalization of a gadolinium complex in the apoferritin cavity: A route to obtain high relaxivity contrast agents for magnetic resonance imaging. *Angewandte Chemie International Edition*, 41(6), 1017–1019.
3. Almeida, A. V., Carvalho, A. J., & Pereira, A. S. (2021). Encapsulin nanocages: Protein encapsulation and iron sequestration. *Coordination Chemistry reviews*, 448, 214188.
4. Anderson, L. J. ;Lee, J., Mallen, M. C., Migula, D. ;Liu, H., Wu, P. C. ; Dash, A., et al. (2021). Evaluation of physical function and its association with body composition, quality of life and biomarkers in cancer cachexia patients. *Clinical Nutrition*, 40(3), 978–986.
5. Artiukhov, A. V., Pometun, A. A., Zubanova, S. A., Tishkov, V. I., & Bunik, V. I. (2020). Advantages of formate dehydrogenase reaction for efficient NAD⁺ quantification in biological samples. *Analytical Biochemistry*, 603, 113797.
6. Ashley, C. E.; Dunphy, D. R., Jiang, Z., Carnes, E. C.; Yuan, Z., Petsev, D. N., Atanasov, P. B.; Velez, O. D.; Sprung, M.; Wang, J. Convective Assembly of 2D Lattices of Virus-like Particles Visualized by In-Situ Grazing-Incidence Small-Angle X-Ray Scattering. *Small* 2011, 7 (8), 1043-1050.
7. Aussignargues, C., Pandelia, M.-E., Sutter, M., Plegaria, J. S., Zarzycki, J., Turmo, A., Huang, J., et al. (2016). Structure and Function of a Bacterial Microcompartment Shell Protein Engineered to Bind a [4Fe-4S] Cluster. *Journal of the American Chemical Society*, 138(16), 5262–5270.
8. Azuma, Y., Edwardson, T. G. W., Terasaka, N., & Hilvert, D. (2018). Modular Protein Cages for Size-Selective RNA Packaging *in vivo*. *Journal of the American Chemical Society*, 140(2), 566–569.
9. Azuma, Y., Zschoche, R., Tinzl, M., & Hilvert, D. Quantitative Packaging of Active Enzymes Into a Protein Cage. *Angew. Chem. Int. Edit.* 2016, 55(4), 1531-1534.
10. Azuma, Y., Zschoche, R., & Hilvert, D. (2017). The C-terminal peptide of Aquifex aeolicus riboflavin synthase directs encapsulation of native and foreign guests by a cage-forming lumazine synthase. *The Journal of Biological Chemistry*, 292(25), 10321–10327.
11. Azuma, Y., Zschoche, R., Tinzl, M., & Hilvert, D. (2016). Quantitative Packaging of Active Enzymes into a Protein Cage. *Angewandte Chemie International Edition*, 55(4), 1531–1534.
12. Basu, R., Zhai, L., Rosso, B., & Tumban, E. (2020). Bacteriophage Q β virus-like particles displaying Chikungunya virus B-cell epitopes elicit high-titer E2 protein antibodies but fail to neutralize a Thailand strain of Chikungunya virus. *Vaccine*, 38(11), 2542–2550.
13. Baykalir, Y., & Simsek, U. G. (2018). Impact of different rearing systems and age on bovans white layer's performance, egg quality traits and synthesis of heat shock protein 70 kda. *Annals of Animal Science*, 18(4), 1045–1060.

14. Ben, J., Jiang, B., Wang, D., Liu, Q., Zhang, Y., Qi, Y., Tong, X., et al. (2019). Major vault protein suppresses obesity and atherosclerosis through inhibiting IKK-NF- κ B signaling mediated inflammation. *Nature Communications*, 10(1), 1801.
15. Betancor, L., & Luckarift, H. R. (2008). Bioinspired enzyme encapsulation for biocatalysis. *Trends in Biotechnology*, 26(10), 566–572.
16. Beyeh, N. K., Nonappa, Liljeström, V., Mikkilä, J., Korpi, A., Bochicchio, D., Pavan, G. M., et al. (2018). Crystalline Cyclophane-Protein Cage Frameworks. *ACS Nano*, 12(8), 8029–8036.
17. Bhattacharya, P., Du, D., & Lin, Y. (2014). Bioinspired nanoscale materials for biomedical and energy applications. *Journal of the Royal Society, Interface*, 11(95), 20131067.
18. Bock, F. J., & Tait, S. W. G. (2020). Mitochondria as multifaceted regulators of cell death. *Nature Reviews. Molecular Cell Biology*, 21(2), 85–100.
19. Boeckx, J., Hertog, M., Geeraerd, A., & Nicolai, B. (2017). Kinetic modelling: an integrated approach to analyze enzyme activity assays. *Plant Methods*, 13, 69.
20. Bommarius, A. S., Schwarm, M., Stingl, K., Kottenhahn, M., Huthmacher, K., & Drauz, K. (1995). Synthesis and use of enantiomerically pure tert-leucine. *Tetrahedron: Asymmetry*, 6(12), 2851–2888.
21. Boyer, C., Bulmus, V., Liu, J., Davis, T. P., Stenzel, M. H., & Barner-Kowollik, C. (2007). Well-defined protein-polymer conjugates via in situ RAFT polymerization. *Journal of the American Chemical Society*, 129(22), 7145–7154.
22. Brumbarova, T., & Ivanov, R. (2016). Differential gene expression and protein phosphorylation as factors regulating the state of the arabidopsis SNX1 protein complexes in response to environmental stimuli. *Frontiers in Plant Science*, 7, 1456.
23. Buchholz, C. J., Friedel, T., & Büning, H. (2015). Surface-Engineered Viral Vectors for Selective and Cell Type-Specific Gene Delivery. *Trends in Biotechnology*, 33(12), 777–790.
24. Calcines-Cruz, C., Finkelstein, I. J., & Hernandez-Garcia, A. (2021). CRISPR-Guided Programmable Self-Assembly of Artificial Virus-Like Nucleocapsids. *Nano Letters*, 21(7), 2752–2757.
25. Cameron, J. C.; Wilson, S. C.; Bernstein, S. L.; & Kerfeld, C. A., Biogenesis of a bacterial organelle: The Carboxysome Assembly Pathway. *Cell* (2013), 155 (5), 1131-1140.
26. Cannon, K. A., Park, R. U., Boyken, S. E., Nattermann, U., Yi, S., Baker, D., King, N. P., et al. (2020). Design and structure of two new protein cages illustrate successes and ongoing challenges in protein engineering. *Protein Science*, 29(4), 919–929.
27. Carter, J. L. L., Bekhouche, M., Noiriél, A., Blum, L. J., & Doumèche, B. (2014). Directed evolution of a formate dehydrogenase for increased tolerance to ionic liquids reveals a new site for increasing the stability. *Chembiochem*, 15(18), 2710–2718.
28. Caruso, F., Trau, D., Möhwald, H., & Renneberg, R. (2000). Enzyme Encapsulation in Layer-by-Layer Engineered Polymer Multilayer Capsules. *Langmuir: the ACS Journal of Surfaces and Colloids*, 16(4), 1485–1488.
29. Casini, G. L., Graham, D., Heine, D., Garcea, R. L., & Wu, D. T. (2004). *In vitro* papillomavirus capsid assembly analyzed by light scattering. *Virology*, 325(2), 320–327.
30. Ceccarelli, C., Liang, Z.-X., Strickler, M., Prehna, G., Goldstein, B. M., Klinman, J. P., & Bahnson, B. J. (2004). Crystal structure and amide H/D exchange of binary complexes of

- alcohol dehydrogenase from *Bacillus stearothermophilus*: Insight into thermostability and cofactor binding. *Biochemistry*, 43(18), 5266–5277.
31. Chabeda, A., van Zyl, A. R., Rybicki, E. P., & Hitzeroth, I. I. (2019). Substitution of Human Papillomavirus Type 16 L2 Neutralizing Epitopes Into L1 Surface Loops: The Effect on Virus-Like Particle Assembly and Immunogenicity. *Frontiers in Plant Science*, 10, 779.
 32. Chakraborti, S., Korpi, A., Kumar, M., Stępień, P., Kostianen, M. A., & Heddle, J. G. (2019). Three-Dimensional Protein Cage Array Capable of Active Enzyme Capture and Artificial Chaperone Activity. *Nano Letters*, 19(6), 3918–3924.
 33. Chen, Y., Li, P., Noh, H., Kung, C.-W., Buru, C. T., Wang, X., Zhang, X., et al. (2019). Stabilization of Formate Dehydrogenase in a Metal-Organic Framework for Bioelectrocatalytic Reduction of CO₂. *Angewandte Chemie International Edition*, 58(23), 7682–7686.
 34. Cheng-Chung Lee, Tzu-Ping Ko, Meng-Shiu Lee, Chia-Cheng Chou, Su-Yuan Lai, Andrew H.-J. Wang and Ming-Ying Wang. (n.d.). Purification, crystallization and preliminary X-ray analysis of immunogenic virus-like particles formed by infectious bursal disease virus (IBDV) structural protein VP2. *Acta Crystallographica. Sect. D, Biological Crystallography*.
 35. Chiou, B., & Connor, J. R. (2018). Emerging and dynamic biomedical uses of ferritin. *Pharmaceuticals (Basel, Switzerland)*, 11(4).
 36. Chowdhury, C., Chun, S., Pang, A., Sawaya, M. R., Sinha, S., Yeates, T. O., & Bobik, T. A. (2015). Selective molecular transport through the protein shell of a bacterial microcompartment organelle. *Proceedings of the National Academy of Sciences of the United States of America*, 112(10), 2990–2995.
 37. Chowdhury, C., Sinha, S., Chun, S., Yeates, T. O., & Bobik, T. A. (2014). Diverse bacterial microcompartment organelles. *Microbiology and Molecular Biology Reviews*, 78(3), 438–468.
 38. Chowdhury, C.; Sinha, S.; Chun, S.; Yeates, T. O.; & Bobik, T. A., (2014) Diverse Bacterial Microcompartment Organelles. *Microbiology and Molecular Biology Reviews* 2014, 78 (3), 438-468.
 39. Cohen, S., Nathan, J. A., & Goldberg, A. L. (2015). Muscle wasting in disease: molecular mechanisms and promising therapies. *Nature Reviews. Drug Discovery*, 14(1), 58–74.
 40. Collett, S., Torresi, J., Silveira, L. E., Truong, V. K., Christiansen, D., Tran, B. M., Vincan, E., et al. (2021). Investigating virus-host cell interactions: Comparative binding forces between hepatitis C virus-like particles and host cell receptors in 2D and 3D cell culture models. *Journal of Colloid and Interface Science*, 592, 371–384.
 41. Comellas-Aragones, M.; Engelkamp, H.; Claessen, V. I.; Sommerdijk, N. A. J. M.; Rowan, A. E.; Christianen, P. C. M.; Maan, J. C.; Verduin, B. J. M.; Cornelissen, J. J. L. M. & Nolte, R. J. M., (2007) A virus-based single-enzyme nanoreactor. *Nat. Nanotechnol.* 2007, 2 (10), 635-639.
 42. ContentServer.asp.pdf. (n.d.). .
 43. Cristie-David, A. S., Koldewey, P., Meinen, B. A., Bardwell, J. C. A., & Marsh, E. N. G. (2018). Elaborating a coiled-coil-assembled octahedral protein cage with additional protein domains. *Protein Science*, 27(11), 1893–1900.
 44. Dibenedetto, A.; Stufano, P.; Macyk, W.; Baran, T.; Fragale, C.; Costa, M. & Aresta, M., (2012). Hybrid Technologies for an Enhanced Carbon Recycling Based on the Enzymatic

Reduction of CO₂ to Methanol in Water: Chemical and Photochemical NADH Regeneration. *Chemsuschem* 2012, 5 (2), 373-378.

45. Dóka, É., Ida, T., Dagnell, M., Abiko, Y., Luong, N. C., Balog, N., Takata, T., et al. (2020). Control of protein function through oxidation and reduction of persulfidated states. *Science Advances*, 6(1), eaax8358.
46. Douglas, T., & Young, M. (1998). Host–guest encapsulation of materials by assembled virus protein cages. *Nature*, 393(6681), 152–155.
47. Douglas, T., & Young, M. (2006). Viruses: Making friends with old foes. *Science*, 312(5775), 873–875.
48. Duda, R. L., Martincic, K., & Hendrix, R. W. (1995). Genetic basis of bacteriophage HK97 prohead assembly. *Journal of Molecular Biology*, 247(4), 636–647.
49. Edwardson, T. G. W., Levasseur, M. D., Tetter, S., Steinauer, A., Hori, M., & Hilvert, D. (2022). Protein cages: From fundamentals to advanced applications. *Chemical Reviews*, 122(9), 9145–9197.
50. Edwardson, T. G., & Hilvert, D. (2019). Virus-inspired function in engineered protein cages. *Journal of the American Chemical Society*, 141(24), 9432-9443.
51. Endres, D., Miyahara, M., Moisan, P., & Zlotnick, A. (2005). A reaction landscape identifies the intermediates critical for self-assembly of virus capsids and other polyhedral structures. *Protein Science*, 14(6), 1518–1525.
52. Fabian C Herbert, Olivia Brohlin, Tyler Galbraith, Candace Benjamin, Cesar A Reyes, Michael A Luzuriaga, Arezoo Shahrivarkevishahi, & Jeremiah J Gassensmith. (2020) "Supramolecular Encapsulation of Small-Ultra Red Fluorescent Proteins in Virus-Like Nanoparticles for Non-Invasive In Vivo Imaging Agents." *ChemRxiv* (2020): ChemRxiv, 2020. Web.
53. Fan, C.; Cheng, S.; Liu, Y.; Escobar, C. M.; Crowley, C. S.; Jefferson, R. E.; Yeates, T. O. & Bobik, T. A.,(2010). Short N-terminal sequences package proteins into bacterial microcompartments. *Proceedings of the National Academy of Sciences* 2010, 107 (16), 7509-7514.
54. Fan, C.; Cheng, S.; Sinha, S.; & Bobik, T. A., (2012). Interactions between the termini of lumen enzymes and shell proteins mediate enzyme encapsulation into bacterial microcompartments. *Proceedings of the National Academy of Sciences* 2012, 109 (37), 14995-15000.
55. Fan, K., Cao, C., Pan, Y., Lu, D., Yang, D., Feng, J., Song, L., et al. (2012). Magnetoferritin nanoparticles for targeting and visualizing tumour tissues. *Nature Nanotechnology*, 7(7), 459–464.
56. Fiedler, J. D., Brown, S. D., Lau, J. L., & Finn, M. G. (2010). RNA-directed packaging of enzymes within virus-like particles. *Angewandte Chemie International Edition*, 49(50), 9648–9651.
57. Fiedler, J. D.; Brown, S. D.; Lau, J. L. & Finn, M. G. (2010) RNA-Directed Packaging of Enzymes within Virus-like Particles. *Angew. Chem. Int. Edit.* 2010, 49 (50), 9648-9651.
58. Frank, S.; Lawrence, A. D.; Prentice, M. B. & Warren, M. J. (2013). Bacterial microcompartments moving into a synthetic biological world. *J. Biotechnol.* 2013, 163 (2), 273-279.
59. Freeman, A. (2017). Protein-Mediated Biotemplating on the Nanoscale. *Biomimetics*, 2(3), 14.

60. Frohlich, P.; Albert, K. & Bertau, M. (2017). Formate dehydrogenase - a biocatalyst with novel applications in organic chemistry. *Org Biomol Chem* 2011, 9 (22), 7941-7950.
61. Fuenmayor, J., Gòdia, F., & Cervera, L. (2017). Production of virus-like particles for vaccines. *New Biotechnology*, 39(Pt B), 174–180.
62. Gabashvili, A. N., Chmelyuk, N. S., Efremova, M. V., Malinovskaya, J. A., Semkina, A. S., & Abakumov, M. A. (2020). Encapsulins-Bacterial Protein Nanocompartments: Structure, Properties, and Application. *Biomolecules*, 10(6).
63. Ganganboina, A. B., & Doong, R. (2018). The biomimic oxidase activity of layered V2O5 nanozyme for rapid and sensitive nanomolar detection of glutathione. *Sensors and Actuators B: Chemical*, 273, 1179–1186.
64. Gast, M., Kadzioch, N. P., Milius, D., Origgi, F., & Plattet, P. (2021). Oligomerization and cell egress controlled by two microdomains of canine distemper virus matrix protein. *mSphere*, 6(2).
65. Genes, Proteins, Structures, & Maturation, D. N. A. (n.d.). Mechanism of Head Assembly and DNA Encapsulation in Salmonella Phage P22.
66. Giessen, T. W. & Silver, P. A. A Catalytic Nanoreactor Based on *in vivo* Encapsulation of Multiple Enzymes in an Engineered Protein Nanocompartment. *ChemBioChem* 2016, 17 (20), 1931 – 1935
67. Giessen, T. W., & Silver, P. A. (2016). A catalytic nanoreactor based on *in vivo* encapsulation of multiple enzymes in an engineered protein nanocompartment. *Chembiochem*, 17(20), 1931–1935.
68. Glasgow, Jeff E, Stacy L Capehart, Matthew B Francis, & Danielle Tullman-Ercek. (2012). "Osmolyte-Mediated Encapsulation of Proteins inside MS2 Viral Capsids." *ACS Nano* 6.10 (2012): 8658-664. Web.
69. Grover, G. N., Alconcel, S. N. S., Matsumoto, N. M., & Maynard, H. D. (2009). Trapping of Thiol Terminated Acrylate Polymers with Divinyl Sulfone to Generate Well-Defined Semi-Telechelic Michael Acceptor Polymers. *Macromolecules*, 42(20), 7657–7663.
70. Guo, Q.; Gakhar, L.; Wickersham, K.; Francis, K.; Vardi-Kilshtain, A.; Major, D. T.; Cheatum, & C. M.; Kohen, A. (2016) Structural and kinetic studies of formate dehydrogenase from *Candida boidinii*. *Biochemistry* 2016, 55 (19), 2760-2771.
71. Hale, A. D., Crawford, S. E., Ciarlet, M., Green, J., Gallimore, C., Brown, D. W., Jiang, X., et al. (1999). Expression and self-assembly of Grimsby virus: Antigenic distinction from Norwalk and Mexico viruses. *Clinical and Diagnostic Laboratory Immunology*, 6(1), 142–145.
72. Han, J.-A., Kang, Y. J., Shin, C., Ra, J.-S., Shin, H.-H., Hong, S. Y., Do, Y., et al. (2014). Ferritin protein cage nanoparticles as versatile antigen delivery nanoplatforams for dendritic cell (DC)-based vaccine development. *Nanomedicine : Nanotechnology, biology, and medicine*, 10(3), 561–569.
73. Hanslip, S. J., Zaccai, N. R., Middelberg, A. P. J., & Falconer, R. J. (2006). Assembly of human papillomavirus type-16 virus-like particles: Multifactorial study of assembly and competing aggregation. *Biotechnology Progress*, 22(2), 554–560.
74. Hartmann, T., & Leimkühler, S. (2013). The oxygen-tolerant and NAD⁺-dependent formate dehydrogenase from *Rhodobacter capsulatus* is able to catalyze the reduction of CO₂ to formate. *The FEBS Journal*, 280(23), 6083–6096.

75. Heddle, J. G., Chakraborti, S., & Iwasaki, K. (2017). Natural and artificial protein cages: Design, structure and therapeutic applications. *Current Opinion in Structural Biology*, 43, 148–155.
76. Helgstrand, C., Wikoff, W. R., Duda, R. L., Hendrix, R. W., Johnson, J. E., & Liljas, L. (2003). The refined structure of a protein catenane: The HK97 bacteriophage capsid at 3.44 Å resolution. *Journal of Molecular Biology*, 334(5), 885–899.
77. Heredia, K. L., Bontempo, D., Ly, T., Byers, J. T., Halstenberg, S., & Maynard, H. D. (2005). In situ preparation of protein-"smart" polymer conjugates with retention of bioactivity. *Journal of the American Chemical Society*, 127(48), 16955–16960.
78. Herbert, F. C., O. R Brohlin, T. Galbraith, C. Benjamin, C. A. Reyes, M. A. Luzuriaga, A. Shahrivarkevishahi, & J. J. Gassensmith. (2020) "Supramolecular Encapsulation of Small-Ultrared Fluorescent Proteins in Virus-Like Nanoparticles for Noninvasive In Vivo Imaging Agents." *Bioconjugate Chemistry* 31.5 (2020): 1529-536. Web.
79. Hong, H., Lim, D., Kim, G.-J., Park, S.-H., Sik Kim, H., Hong, Y., Choy, H. E., et al. (2014). Targeted deletion of the ara operon of *Salmonella typhimurium* enhances L-arabinose accumulation and drives PBAD-promoted expression of anti-cancer toxins and imaging agents. *Cell Cycle*, 13(19), 3112–3120.
80. Höpner, T. & Trautwein, A. (1972), Some properties of formate dehydrogenase. *Zeitschrift für Naturforschung B* 1972, 27 (9), 1075-1076.
81. Hortsch, R., & Weuster-Botz, D. (2011). Growth and recombinant protein expression with *Escherichia coli* in different batch cultivation media. *Applied Microbiology and Biotechnology*, 90(1), 69–76.
82. Huang, J., Xu, J., Tian, L., & Zhong, L. (2014). A thioredoxin reductase and/or thioredoxin system-based mechanism for antioxidant effects of ambroxol. *Biochimie*, 97, 92–103.
83. Huang, Z., Elkin, G., Maloney, B. J., Beuhner, N., Arntzen, C. J., Thanavala, Y., & Mason, H. S. (2005). Virus-like particle expression and assembly in plants: hepatitis B and Norwalk viruses. *Vaccine*, 23(15), 1851–1858.
84. Huertas-Díaz, M. C., Phan, S., Elson, A., Nuñez, I., Wei, H., Sakamoto, K., & He, B. (2019). Parainfluenza virus 5 (PIV5) amplifying virus-like particles expressing respiratory syncytial virus (RSV) antigens protect mice against RSV infection. *Vaccine*, 37(22), 2925–2934.
85. Ibraheem, D., Elaissari, A., & Fessi, H. (2014). Administration strategies for proteins and peptides. *International Journal of Pharmaceutics*, 477(1–2), 578–589.
86. Inoue, T.; Kawano, M. A.; Takahashi, R. U.; Tsukarnoto, H.; Enornoto, T.; Imai, T.; Kataoka, K. & Handa, H. (2008). Engineering of SV40-based nano-capsules for delivery of heterologous proteins as fusions with the minor capsid proteins VP2/3. *J. Biotechnol.* 2008, 134 (1-2), 181-192.
87. Jeevanandam, J., Barhoum, A., Chan, Y. S., Dufresne, A., & Danquah, M. K. (2018). Review on nanoparticles and nanostructured materials: history, sources, toxicity and regulations. *Beilstein Journal of Nanotechnology*, 9, 1050–1074.
88. Jiang, L., Cai, W., Tang, F., Wang, Z., & Liu, Y. (2021). Characterization of Fitness Cost Caused by Tigecycline-Resistance Gene tet(X6) in Different Host Bacteria. *Antibiotics* (Basel, Switzerland), 10(10).

89. Jiang, M., & Guo, Z. (2007). Effects of macromolecular crowding on the intrinsic catalytic efficiency and structure of enterobactin-specific isochorismate synthase. *Journal of the American Chemical Society*, 129(4), 730–731.
90. Jiang, M.; & Guo, Z. (2007). Effects of Macromolecular Crowding on the Intrinsic Catalytic Efficiency and Structure of Enterobactin Specific Isochorismate Synthase. *Journal of the American Chemical Society* 2007, 129(4), 730-731.
91. Johnson, J. E., & Chiu, W. (2007). DNA packaging and delivery machines in tailed bacteriophages. *Current Opinion in Structural Biology*, 17(2), 237–243.
92. Johnson, J. E., & Olson, A. J. (2021). Icosahedral virus structures and the protein data bank. *The Journal of Biological Chemistry*, 296, 100554.
93. Jordan, P. C., Patterson, D. P., Saboda, K. N., Edwards, E. J., Miettinen, H. M., Basu, G., Thielges, M. C., et al. (2016). Self-assembling biomolecular catalysts for hydrogen production. *Nature Chemistry*, 8(2), 179–185.
94. Kalarickal, N. C., Rimmer, S., Sarker, P., & Leroux, J.-C. (2007). Thiol-Functionalized Poly(ethylene glycol)- b -polyesters: Synthesis and Characterization. *Macromolecules*, 40(6), 1874–1880.
95. Kerfeld, C. A., Aussignargues, C., Zarzycki, J., Cai, F., & Sutter, M. (2018). Bacterial microcompartments. *Nature Reviews. Microbiology*, 16(5), 277–290.
96. Kerfeld, C. A.; Aussignargues, C.; Zarzycki, J.; Cai, F. & Sutter, M. (2018). Bacterial microcompartments. *Nature Reviews Microbiology* 2018, 16 (5), 277-290.
97. Kerfeld, C. A.; Heinhorst, S.; & Cannon, G. C. (2010). Bacterial microcompartments. *Annual review of microbiology* 2010, 64, 391-408.
98. Kianfar, E. (2021). Protein nanoparticles in drug delivery: Animal protein, plant proteins and protein cages, albumin nanoparticles. *Journal of Nanobiotechnology*, 19(1), 1-32.
99. Kianfar, E. (2021). Protein nanoparticles in drug delivery: Animal protein, plant proteins and protein cages, albumin nanoparticles. *Journal of Nanobiotechnology*, 19(1), 159.
100. Kickhoefer, V. A.; Garcia, Y.; Mikyias, Y.; Johansson, E.; Zhou, J. C.; Raval-Fernandes, S.; Minoofar, P.; Zink, J. I.; Dunn, B.; Stewart, P. L. & Rome, L. H. (2005). Engineering of vault nanocapsules with enzymatic and fluorescent properties. *P Natl Acad Sci USA* 2005, 102 (12), 4348-4352.
101. Kim, H., Choi, H., Bae, Y., & Kang, S. (2019). Development of target-tunable P22 VLP-based delivery nanoplatfoms using bacterial superglue. *Biotechnology and Bioengineering*, 116(11), 2843–2851.
102. Kim, M. H., Park, S., Kim, Y. H., Won, K., & Lee, S. H. (2013). Immobilization of formate dehydrogenase from *Candida boidinii* through cross-linked enzyme aggregates. *Journal of Molecular Catalysis B: Enzymatic*, 97, 209–214.
103. Kim, M. K., Jernigan, R. L., & Chirikjian, G. S. (2003). An elastic network model of HK97 capsid maturation. *Journal of Structural Biology*, 143(2), 107–117.
104. King, J.; Botstein, D.; Casjens, S.; Earnshaw, W.; Harrison, S. & Lenk, E. (1976) . Structure and Assembly of Capsid of Bacteriophage – P22. *Philos. Trans. R. Soc. Lond. Ser. B-Biol. Sci.* 1976, 276 (943), 37-&.
105. Klem, R., de Ruiter, M. V., & Cornelissen, J. J. L. M. (2018). Protecting Encapsulin Nanoparticles with Cysteine-Knot Miniproteins. *Molecular Pharmaceutics*, 15(8), 2991–2996.

106. Kraj, P., Selivanovitch, E., Lee, B., & Douglas, T. (2021). Polymer Coatings on Virus-like Particle Nanoreactors at Low Ionic Strength-Charge Reversal and Substrate Access. *Biomacromolecules*, 22(5), 2107–2118.
107. Kuwabata, S.; Tsuda, R.; Nishida, K. & Yoneyama, H. (1993) Electrochemical Conversion of Carbon-Dioxide to Methanol with Use of Enzymes as Biocatalysts. *Chem Lett* 1993, (9), 1631-1634.
108. Kuwabata, S.; Tsuda, R. & Yoneyama, H. (1994) Electrochemical Conversion of Carbon-Dioxide to Methanol with the Assistance of Formate Dehydrogenase and Methanol Dehydrogenase as Biocatalysts. *J Am Chem Soc* 1994, 116 (12), 5437-5443.
109. Labrou, , N. E. & Rigden, D. J. (2001). Active-site characterization of *Candida boidinii* formate dehydrogenase. *Biochem J* 2001, 354 (2), 455-463.
110. Ladenstein, R., & Morgunova, E. (2020). Second career of a biosynthetic enzyme: Lumazine synthase as a virus-like nanoparticle in vaccine development. *Biotechnology reports (Amsterdam, Netherlands)*, 27, e00494.
111. Lauria, I., Dickmeis, C., Röder, J., Beckers, M., Rütten, S., Lin, Y. Y., Commandeur, U., et al. (2017). Engineered Potato virus X nanoparticles support hydroxyapatite nucleation for improved bone tissue replacement. *Acta Biomaterialia*, 62, 317–327.
112. Laviano, A., Koverech, A., & Mari, A. (2015). Cachexia: clinical features when inflammation drives malnutrition. *The Proceedings of the Nutrition Society*, 74(4), 348–354.
113. Le, D. T., Radukic, M. T., & Müller, K. M. (2019). Adeno-associated virus capsid protein expression in *Escherichia coli* and chemically defined capsid assembly. *Scientific Reports*, 9(1), 18631.
114. Lee, S. K.; Chou, H. H.; Pflieger, B. F.; Newman, J. D.; Yoshikuni, Y. & Keasling, J. D. (2007). Directed evolution of AraC for improved compatibility of arabinose- and lactose-inducible promoters. *Appl Environ Microb* 2007, 73 (18), 5711-5715.
115. Lehuédé, C., Li, X., Dauvillier, S., Vaysse, C., Franchet, C., Clement, E., Esteve, D., et al. (2019). Adipocytes promote breast cancer resistance to chemotherapy, a process amplified by obesity: role of the major vault protein (MVP). *Breast Cancer Research*, 21(1), 7.
116. Liepold, L., Anderson, S., Willits, D., Oltrogge, L., Frank, J. A., Douglas, T., & Young, M. (2007). Viral capsids as MRI contrast agents. *Magnetic Resonance in Medicine*, 58(5), 871–879.
117. Lim, H. A. (2011) Fundamental relationship between operon organization and gene expression. *Proceedings of the National Academy of Sciences* 2011, 108 (26), 10626-10631.
118. Liu, A., de Ruiter, M. V., Zhu, W., Maassen, S. J., Yang, L., & Cornelissen, J. J. L. M. (2018). Compartmentalized Thin Films with Customized Functionality via Interfacial Cross-linking of Protein Cages. *Advanced Functional Materials*, 28(34), 1801574.
119. Liu, Y. C., Grusovin, J., & Adams, T. E. (2018). Electrostatic Interactions between Hendra Virus Matrix Proteins Are Required for Efficient Virus-Like-Particle Assembly. *Journal of Virology*, 92(13).

120. Lu, W., Zhao, Z., Huang, Y.-W., & Wang, B. (2022). Review: A systematic review of virus-like particles of coronavirus: Assembly, generation, chimerism and their application in basic research and in the clinic. *International Journal of Biological Macromolecules*, 200, 487–497.
121. Lua, L. H. L., Connors, N. K., Sainsbury, F., Chuan, Y. P., Wibowo, N., & Middelberg, A. P. J. (2014). Bioengineering virus-like particles as vaccines. *Biotechnology and Bioengineering*, 111(3), 425–440.
122. Ma, J., Liu, J., Zheng, L., Wang, C., Zhao, Q., & Huo, Y. (2022). Sequence addition to the N- or C-terminus of the major capsid protein VP1 of norovirus affects its cleavage and assembly into virus-like particles. *Microbial Pathogenesis*, 169, 105633.
123. Matsumoto, N. M., Prabhakaran, P., Rome, L. H., & Maynard, H. D. (2013). Smart vaults: Thermally-responsive protein nanocapsules. *ACS Nano*, 7(1), 867–874.
124. McClements, D. J. (2018). Encapsulation, protection, and delivery of bioactive proteins and peptides using nanoparticle and microparticle systems: A review. *Advances in Colloid and Interface Science*, 253, 1–22.
125. McConnell, S. A., Cannon, K. A., Morgan, C., McAllister, R., Amer, B. R., Clubb, R. T., & Yeates, T. O. (2020). Designed protein cages as scaffolds for building multienzyme materials. *ACS Synthetic Biology*, 9(2), 381–391.
126. McConnell, S. A., Cannon, K. A., Morgan, C., McAllister, R., Amer, B. R., Clubb, R. T., & Yeates, T. O. (2020). Designed protein cages as scaffolds for building multienzyme materials. *ACS Synthetic Biology*, 9(2), 381–391.
127. McCoy, K., Selivanovitch, E., Luque, D., Lee, B., Edwards, E., Castón, J. R., & Douglas, T. (2018). Cargo Retention inside P22 Virus-Like Particles. *Biomacromolecules*, 19(9), 3738–3746.
128. Miermont, A.; Barnhill, H.; Strable, E.; Lu, X. W.; Wall, K. A.; Wang, Q.; Finn, M. G. & Huang, X. F. (2008). Cowpea mosaic virus capsid: A promising carrier for the development of carbohydrate based antitumor Vaccines. *Chem-Eur J* 2008, 14 (16), 4939-4947.
129. Minten, I. J., Hendriks, L. J. A., Nolte, R. J. M., & Cornelissen, J. J. L. M. (2009). Controlled encapsulation of multiple proteins in virus capsids. *Journal of the American Chemical Society*, 131(49), 17771–17773.
130. Minten, I. J.; Claessen, V. I.; Blank, K.; Rowan, A. E.; Nolte, R. J. M. & Cornelissen, J. J. L. M. (2011). Catalytic capsids: the art of confinement. *Chem. Sci.* 2011, 2 (2), 358-362.
131. Mohsen, M. O., Augusto, G., & Bachmann, M. F. (2020). The 3Ds in virus-like particle based-vaccines: “Design, Delivery and Dynamics”. *Immunological Reviews*, 296(1), 155–168.
132. Mohsen, M. O., Speiser, D. E., Knuth, A., & Bachmann, M. F. (2020). Virus-like particles for vaccination against cancer. *Wiley Interdisciplinary Reviews. Nanomedicine and Nanobiotechnology*, 12(1), e1579.
133. Moisant, P., Neeman, H., & Zlotnick, A. (2010). Exploring the paths of (virus) assembly. *Biophysical Journal*, 99(5), 1350–1357.
134. Morgunova, E., Saller, S., Haase, I., Cushman, M., Bacher, A., Fischer, M., & Ladenstein, R. (2007). Lumazine synthase from *Candida albicans* as an anti-fungal target enzyme: Structural and biochemical basis for drug design. *The Journal of Biological Chemistry*, 282(23), 17231–17241.

135. Newcomer, R. L., Fraser, L. C. R., Teschke, C. M., & Alexandrescu, A. T. (2015). Mechanism of Protein Denaturation: Partial Unfolding of the P22 Coat Protein I-Domain by Urea Binding. *Biophysical Journal*, 109(12), 2666–2677.
136. Neyroud, D., Nosacka, R. L., Callaway, C. S., Trevino, J. G., Hu, H., Judge, S. M., & Judge, A. R. (2021). FoxP1 is a transcriptional repressor associated with cancer cachexia that induces skeletal muscle wasting and weakness. *Journal of Cachexia, Sarcopenia & Muscle*, 12(2), 421–442.
137. Ng, B. C., Yu, M., Gopal, A., Rome, L. H., Monbouquette, H. G., & Tolbert, S. H. (2008). Encapsulation of semiconducting polymers in vault protein cages. *Nano Letters*, 8(10), 3503–3509.
138. O'Neil, A.; Prevelige, P. E.; Basu, G. & Douglas, T. (2012). Coconfinement of Fluorescent Proteins: Spatially Enforced Communication of GFP and mCherry Encapsulated within the P22 Capsid. *Biomacromolecules* 2012, 13 (12), 3902-3907.
139. O'Neil, A.; Prevelige, P. E.; & Douglas, T. (2013) Stabilizing viral nano-reactors for nerve-agent degradation. *Biomater Sci-Uk* 2013, 1 (8), 881-886.
140. O'Neil, A.; Reichhardt, C.; Johnson, B.; Prevelige, P. E. & Douglas, T. (2011). Genetically Programmed *In vivo* Packaging of Protein Cargo and Its Controlled Release from Bacteriophage P22. *Angew. Chem. Int. Edit.* 2011, 50 (32), 7425-7428.
141. O'Neil, A., Reichhardt, C., Johnson, B., Prevelige, P. E., & Douglas, T. (2011). Genetically programmed *in vivo* packaging of protein cargo and its controlled release from bacteriophage P22. *Angewandte Chemie International Edition*, 50(32), 7425–7428.
142. Obert, R. & Dave, B. C., Enzymatic Conversion of Carbon Dioxide to Methanol: Enhanced Methanol Production in Silica Sol-Gel Matrices. *J Am Chem Soc* 1999, 121 (51), 12192-12193.
143. Olsen, S. N. (2006). Applications of isothermal titration calorimetry to measure enzyme kinetics and activity in complex solutions. *Thermochimica acta*, 448(1), 12–18.
144. Olsen, S. N. (2006). Applications of Isothermal Titration Calorimetry to Measure Enzyme Kinetics and Activity in Complex Solutions. *Thermochim. Acta* 2006, 448, 12–18.
145. Palombo, M., Bonucci, A., Etienne, E., Ciurli, S., Uversky, V. N., Guigliarelli, B., Belle, V., et al. (2017). The relationship between folding and activity in UreG, an intrinsically disordered enzyme. *Scientific Reports*, 7(1), 5977.
146. Paramelle, D., Peng, T., Free, P., Fernig, D. G., Lim, S., & Tomczak, N. (2016). Specific Internalisation of Gold Nanoparticles into Engineered Porous Protein Cages via Affinity Binding. *Plos One*, 11(9), e0162848.
147. Parent, K. N., Khayat, R., Tu, L. H., Suhanovsky, M. M., Cortines, J. R., Teschke, C. M., Johnson, J. E., et al. (2010). P22 coat protein structures reveal a novel mechanism for capsid maturation: Stability without auxiliary proteins or chemical crosslinks. *Structure*, 18(3), 390–401.
148. Parker, M. H., Casjens, S., & Prevelige, P. E. (1998). Functional domains of bacteriophage P22 scaffolding protein. *Journal of Molecular Biology*, 281(1), 69–79.
149. Parker, M. H., Stafford, W. F., & Prevelige, P. E. (1997). Bacteriophage P22 scaffolding protein forms oligomers in solution. *Journal of Molecular Biology*, 268(3), 655–665.
150. Parker, M. H.; Casjens, S. & Prevelige, P. E. (1998). Functional domains of bacteriophage P22 scaffolding protein. *J Mol Biol* 1998, 281 (1), 69-79.

151. Parker, M. H. & Prevelige Jr, P. E. (1998). Electrostatic interactions drive scaffolding/coat protein binding and procapsid maturation in bacteriophage P22. *Virology* 1998, 250 (2), 337-349.
152. Parkinson, B. A. & Weaver, P. F. (1984). Photoelectrochemical Pumping of Enzymatic Co₂ Reduction. *Nature* 1984, 309 (5964), 148-149.
153. Pasotti, L., & Zucca, S. (2014). Advances and computational tools towards predictable design in biological engineering. *Computational and mathematical methods in medicine*, 2014, 369681.
154. Patterson, D. P., Prevelige, P. E., & Douglas, T. (2012). Nanoreactors by programmed enzyme encapsulation inside the capsid of the bacteriophage P22. *ACS Nano*, 6(6), 5000–5009.
155. Patterson, D. P., Schwarz, B., Waters, R. S., Gedeon, T., & Douglas, T. (2014). Encapsulation of an enzyme cascade within the bacteriophage P22 virus-like particle. *ACS Chemical Biology*, 9(2), 359–365.
156. Patterson, D. P., Su, M., Franzmann, T. M., Sciore, A., Skiniotis, G., & Marsh, E. N. G. (2014). Characterization of a highly flexible self-assembling protein system designed to form nanocages. *Protein Science*, 23(2), 190–199.
157. Patterson, D. P.; LaFrance, B. & Douglas, T. (2013). Rescuing Recombinant Proteins by Sequestration into the P22 VLP. *Chem Commun* 2013, 49 (88), 10412-10414.
158. Patterson, D. P.; McCoy, K.; Fijen, C. & Douglas, T. (2014). Constructing Catalytic Antimicrobial Nanoparticles by Encapsulation of Hydrogen Peroxide Producing Enzyme Inside the P22 VLP. *J Mater Chem B* 2014, 2 (36), 5948-5951.
159. Patterson, D. P.; Prevelige, P. E. & Douglas, T. (2012). Nanoreactors by Programmed Enzyme Encapsulation Inside the Capsid of the Bacteriophage P22. *ACS Nano* 2012, 6 (6), 5000-5009.
160. Patterson, D. P.; Rynda-Apple, A.; Harmsen, A. L.; Harmsen, A. G. & Douglas, T. (2013). Biomimetic Antigenic Nanoparticles Elicit Controlled Protective Immune Response to Influenza. *Acs Nano* 2013, 7 (4), 3036-3044.
161. Patterson, D. P.; Schwarz, B.; El-Boubbou, K.; van der Oost, J.; Prevelige, P. E. & Douglas, T. (2012). Virus-Like Particle Nanoreactors: Programmed Encapsulation of the Thermostable CelB Glycosidase Inside the P22 Capsid. *Soft Matter* 2012, 8 (39), 10158-10166.
162. Patterson, D. P.; Schwarz, B.; Waters, R. S.; Gedeon, T. & Douglas, T. (2014). Encapsulation of an Enzyme Cascade within the Bacteriophage P22 Virus-Like Particle. *Acs Chem Biol* 2014, 9 (2), 359-365.
163. Patterson, D., Edwards, E., & Douglas, T. (2015). Hybrid Nanoreactors: Coupling Enzymes and Small-Molecule Catalysts within Virus-Like Particles. *Israel Journal of Chemistry*, 55(1), 96–101.
164. Patterson, D., Schwarz, B., Avera, J., Western, B., Hicks, M., Krugler, P., Terra, M., et al. (2017). Sortase-Mediated Ligation as a Modular Approach for the Covalent Attachment of Proteins to the Exterior of the Bacteriophage P22 Virus-like Particle. *Bioconjugate Chemistry*, 28(8), 2114–2124.
165. Patterson, D.; Edwards, E. & Douglas, T. (2014). Hybrid Nanoreactors: Coupling Enzymes and Small-Molecule Catalysts within Virus-Like Particles. *Israel Journal of Chemistry* 2014.

166. Penna, F., Ballarò, R., Martinez-Cristobal, P., Sala, D., Sebastian, D., Busquets, S., Muscaritoli, M., et al. (2019). Autophagy exacerbates muscle wasting in cancer cachexia and impairs mitochondrial function. *Journal of Molecular Biology*, 431(15), 2674–2686.
167. Perlmutter, J. D., & Hagan, M. F. (2015). Mechanisms of virus assembly. *Annual Review of Physical Chemistry*, 66, 217–239.
168. Perlmutter, J. D., Perkett, M. R., & Hagan, M. F. (2014). Pathways for virus assembly around nucleic acids. *Journal of Molecular Biology*, 426(18), 3148–3165.
169. Pietricola, G., Tommasi, T., Dosa, M., Camelin, E., Berruto, E., Ottone, C., Fino, D., et al. (2021). Synthesis and characterization of ordered mesoporous silicas for the immobilization of formate dehydrogenase (FDH). *International journal of biological macromolecules*, 177, 261–270.
170. Prevelige, P. E., King, J., & Silva, J. L. (1994). Pressure denaturation of the bacteriophage P22 coat protein and its entropic stabilization in icosahedral shells. *Biophysical Journal*, 66(5), 1631–1641.
171. Prevelige, P. E., Thomas, D., & King, J. (1988). Scaffolding protein regulates the polymerization of P22 coat subunits into icosahedral shells *in vitro*. *Journal of Molecular Biology*, 202(4), 743–757.
172. Prevelige, P. E., Thomas, D., & King, J. (1993). Nucleation and growth phases in the polymerization of coat and scaffolding subunits into icosahedral procapsid shells. *Biophysical Journal*, 64(3), 824–835.
173. Putz, M., Lacrama, A.-M., & Ostafe, V. (2006). Full analytic progress curves of enzymic reactions *in vitro*. *International Journal of Marine Science*, 7(11), 469–484.
174. Quax, T. E. F., Claassens, N. J., Söll, D., & van der Oost, J. (2015). Codon Bias as a Means to Fine-Tune Gene Expression. *Molecular Cell*, 59(2), 149–161.
175. Quax, T. E. F., Claassens, N. J., Söll, D., van der Oost, J. Codon Bias as a Means to Fine-Tune Gene Expression. *Molecular Cell* 2015, 59(2), 149–161.
176. Ra, J.-S., Shin, H.-H., Kang, S., & Do, Y. (2014). Lumazine synthase protein cage nanoparticles as antigen delivery nanoplatfroms for dendritic cell-based vaccine development. *Clinical and experimental vaccine research*, 3(2), 227–234.
177. Raj, S. B., Ramaswamy, S., & Plapp, B. V. (2014). Yeast alcohol dehydrogenase structure and catalysis. *Biochemistry*, 53(36), 5791–5803.
178. Reichert, U.; Knieps, E.; Slusarczyk, H.; Kula, M. R. & Thommes, J. (2001). Isolation of a recombinant formate dehydrogenase by pseudo-affinity expanded bed adsorption. *J Biochem Bioph Meth* 2001, 49 (1-3), 533-552.
179. Reichhardt, C.; Uchida, M.; O'Neil, A.; Li, R.; Prevelige, P. E. & Douglas, T. (2011). Templated assembly of organic-inorganic materials using the core shell structure of the P22 bacteriophage. *Chem Commun* 2011, 47 (22), 6326-6328.
180. Ren, H., Zhu, S., & Zheng, G. (2019). Nanoreactor Design Based on Self-Assembling Protein Nanocages. *International Journal of Molecular Sciences*, 20(3).
181. Renggli, K.; Baumann, P.; Langowska, K.; Onaca, O.; Bruns, N. & Meier, W. (2011). Nanoreactors: Selective and Responsive Nanoreactors (*Adv. Funct. Mater.* 7/2011). *Adv. Funct. Mater.* 2011, 21 (7), 1206-1205.
182. Rodriguez, J.-M. G., Hux, N. P., Philips, S. J., & Towns, M. H. (2019). Michaelis–menten graphs, lineweaver–burk plots, and reaction schemes: Investigating

- introductory biochemistry students' conceptions of representations in enzyme kinetics. *Journal of Chemical Education*.
183. Saganuwan, S. A. (2021). Application of modified Michaelis - Menten equations for determination of enzyme inducing and inhibiting drugs. *BMC Pharmacology & Toxicology*, 22(1), 57.
 184. Sakaguchi, M., Mukaeda, H., Kume, A., Toyoda, Y., Sakoh, T., & Kawakita, M. (2021). Evaluation of the roles of hydrophobic residues in the N-terminal region of archaeal trehalase in its folding. *Applied Microbiology and Biotechnology*, 105(8), 3181–3194.
 185. Sánchez-Rodríguez, S. P., Münch-Anguiano, L., Echeverría, O., Vázquez-Nin, G., Mora-Pale, M., Dordick, J. S., & Bustos-Jaimes, I. (2012). Human parvovirus B19 virus-like particles: *In vitro* assembly and stability. *Biochimie*, 94(3), 870–878.
 186. Sánchez-Sánchez, L., Tapia-Moreno, A., Juárez-Moreno, K., Patterson, D. P., Cadena-Nava, R. D., Douglas, T., & Vazquez-Duhalt, R. (2015). Design of a VLP-nanovehicle for CYP450 enzymatic activity delivery. *Journal of Nanobiotechnology*, 13, 66.
 187. Sano, K.-I., Ajima, K., Iwahori, K., Yudasaka, M., Iijima, S., Yamashita, I., & Shiba, K. (2005). Endowing a ferritin-like cage protein with high affinity and selectivity for certain inorganic materials. *Small (Germany)*, 1(8–9), 826–832.
 188. Saxena, P.; He, L.; Malyutin, A.; Datta, S. A.; Rein, A.; Bond, K. M.; Jarrold, M. F.; Spilotros, A.; Svergun, D. & Douglas, T. (2016). Virus matryoshka: A Bacteriophage Particle—Guided Molecular Assembly Approach to a Monodisperse Model of the Immature Human Immunodeficiency Virus. *Small* 2016, 12 (42), 5862-5872.
 189. Schenk, A. S.; Eiben, S.; Goll, M.; Reith, L.; Kulak, A. N.; Meldrum, F. C.; Jeske, H.; Wege, C. & Ludwigs, S. (2017). Virus-directed formation of electrocatalytically active nanoparticle-based Co₃O₄ tubes. *Nanoscale* 2017, 9 (19), 6334-6345.
 190. Schoonen, L., Eising, S., van Eldijk, M. B., Bresseleers, J., van der Pijl, M., Nolte, R. J. M., Bongers, K. M., et al. (2018). Modular, Bioorthogonal Strategy for the Controlled Loading of Cargo into a Protein Nanocage. *Bioconjugate Chemistry*, 29(4), 1186–1193.
 191. Schwarz, B., Madden, P., Avera, J., Gordon, B., Larson, K., Miettinen, H. M., Uchida, M., et al. (2015). Symmetry Controlled, Genetic Presentation of Bioactive Proteins on the P22 Virus-like Particle Using an External Decoration Protein. *ACS Nano*, 9(9), 9134–9147.
 192. Sciore, A., Su, M., Koldewey, P., Eschweiler, J. D., Diffley, K. A., Linhares, B. M., Ruotolo, B. T., et al. (2016). Flexible, symmetry-directed approach to assembling protein cages. *Proceedings of the National Academy of Sciences of the United States of America*, 113(31), 8681–8686.
 193. Selivanovitch, E., Koliyatt, R., & Douglas, T. (2019). Chemically Induced Morphogenesis of P22 Virus-like Particles by the Surfactant Sodium Dodecyl Sulfate. *Biomacromolecules*, 20(1), 389–400.
 194. Servid, A., Jordan, P., O'Neil, A., Prevelige, P., & Douglas, T. (2013). Location of the bacteriophage P22 coat protein C-terminus provides opportunities for the design of capsid-based materials. *Biomacromolecules*, 14(9), 2989–2995.
 195. Sharma, J. & Douglas, T. (2020). Tuning the Catalytic Properties of P22 Nanoreactors Through Compositional Control. *Nanoscale* 2020, 12(1), 336-346.

196. Sharma, J., & Douglas, T. (2020). Tuning the catalytic properties of P22 nanoreactors through compositional control. *Nanoscale*, 12(1), 336–346.
197. Shen, W., Qiu, Y., Li, J., Wu, C., Liu, Z., Zhang, X., Hu, X., et al. (2019). IL-25 promotes cisplatin resistance of lung cancer cells by activating NF- κ B signaling pathway to increase of major vault protein. *Cancer Medicine*, 8(7), 3491–3501.
198. Sigmund, F., Massner, C., Erdmann, P., Stelzl, A., Rolbieski, H., Desai, M., Bricault, S., et al. (2018). Bacterial encapsulins as orthogonal compartments for mammalian cell engineering. *Nature Communications*, 9(1), 1990.
199. Simpson, L. W., Good, T. A., & Leach, J. B. (2020). Protein folding and assembly in confined environments: Implications for protein aggregation in hydrogels and tissues. *Biotechnology Advances*, 42, 107573.
200. Slocik, J. M., Crouse, C. A., Spowart, J. E., & Naik, R. R. (2013). Biologically tunable reactivity of energetic nanomaterials using protein cages. *Nano Letters*, 13(6), 2535–2540.
201. Slusarczyk, H.; Felber, S.; Kula, M. R. & Pohl, M. (2000). Stabilization of NAD-dependent formate dehydrogenase from *Candida boidinii* by Site-Directed Mutagenesis of Cysteine Residues. *Eur J Biochem* 2000, 267 (5), 1280-1289.
202. Slusarczyk, H.; Pohl, M. & Kula, M. R. (1998). Cloning and Stabilization of NAD-dependent Formate Dehydrogenase from *Candida boidinii* by Site-Directed Mutagenesis. *Progr Biotechnol* 1998, 15, 331-336.
203. Solanki, K., Abdallah, W., & Banta, S. (2016). Extreme makeover: Engineering the activity of a thermostable alcohol dehydrogenase (AdhD) from *Pyrococcus furiosus*. *Biotechnology Journal*, 11(12), 1483–1497.
204. Steinmetz, N. F., Findlay, K. C., Noel, T. R., Parker, R., Lomonossoff, G. P., & Evans, D. J. (2008). Layer-by-layer assembly of viral nanoparticles and polyelectrolytes: the film architecture is different for spheres versus rods. *Chembiochem*, 9(10), 1662–1670.
205. Steinmetz, N. F., Lim, S., & Sainsbury, F. (2020). Protein cages and virus-like particles: from fundamental insight to biomimetic therapeutics. *Biomaterials Science*, 8(10), 2771-2777.
206. Stewart, A. M.; Stewart, K. L.; Yeates, T. O. & Bobik, T. A. (2021). Advances in the World of Bacterial Microcompartments. *Trends in Biochemical Sciences* 2021.
207. Stojiljkovic, I.; Bäuml, A. J. & Heffron, F. (1995). Ethanolamine utilization in *Salmonella typhimurium*: nucleotide sequence, protein expression, and mutational analysis of the cchA cchB eutE eutJ eutG eutH gene cluster. *Journal of bacteriology* 1995, 177 (5), 1357-1366.
208. Stupka, I., & Heddle, J. G. (2020). Artificial protein cages - inspiration, construction, and observation. *Current Opinion in Structural Biology*, 64, 66–73.
209. Sun, Q. Y.; Jiang, Y. J.; Jiang, Z. Y.; Zhang, L.; Sun, X. H. & Li, J. (2009). Green and Efficient Conversion of CO₂ to Methanol by Biomimetic Coimmobilization of Three Dehydrogenases in Protamine-Templated Titania. *Ind Eng Chem Res* 2009, 48 (9), 4210-4215.
210. Sun, R., & Lim, S. (2021). Protein cages as building blocks for superstructures. *Engineering Biology*, 5(2), 35–42.
211. Suprenant, K. A. (2002). Vault ribonucleoprotein particles: Sarcophagi, Gondolas, or Safety Deposit Boxes? *Biochemistry*, 41(49), 14447–14454.

212. Sutter, M., Faulkner, M., Aussignargues, C., Paasch, B. C., Barrett, S., Kerfeld, C. A., & Liu, L.-N. (2016). Visualization of Bacterial Microcompartment Facet Assembly Using High-Speed Atomic Force Microscopy. *Nano Letters*, 16(3), 1590–1595.
213. Tanaka, H., & Tsukihara, T. (2012). Structural studies of large nucleoprotein particles, vaults. *Proceedings of the Japan Academy, Series B*, 88(8), 416–433.
214. Tanaka, S.; Kerfeld, C. A.; Sawaya, M. R.; Cai, F.; Heinhorst, S.; Cannon, G. C. & Yeates, T. O. (2008). Atomic-level models of the bacterial carboxysome shell. *Science* 2008, 319 (5866), 1083-1086.
215. Tanaka, S.; Sawaya, M. R. & Yeates, T. O. (2010). Structure and mechanisms of a protein-based organelle in *Escherichia coli*. *Science* 2010, 327 (5961), 81-84.
216. Tellinghuisen, J. (2018). Can you trust the parametric standard errors in nonlinear least squares? Yes, with provisos. *Biochimica et biophysica acta. General Subjects*, 1862(4), 886–894.
217. Terasaka, N., Azuma, Y., & Hilvert, D. (2018). Laboratory evolution of virus-like nucleocapsids from nonviral protein cages. *Proceedings of the National Academy of Sciences of the United States of America*, 115(21), 5432–5437.
218. Teschke, C. M., & Parent, K. N. (2010). “Let the phage do the work”: Using the phage P22 coat protein structures as a framework to understand its folding and assembly mutants. *Virology*, 401(2), 119–130.
219. Tetter, S., & Hilvert, D. (2017). Enzyme encapsulation by a ferritin cage. *Angewandte Chemie International Edition*, 56(47), 14933–14936.
220. Thaker, S. K., Ch’ng, J., & Christofk, H. R. (2019). Viral hijacking of cellular metabolism. *BMC Biology*, 17(1), 59.
221. Thangam, R., Patel, K. D., Kang, H., & Paulmurugan, R. (2021). Advances in Engineered Polymer Nanoparticle Tracking Platforms towards Cancer Immunotherapy- Current Status and Future Perspectives. *Vaccines*, 9(8).
222. Thuman-Commike, P. A., Greene, B., Jakana, J., Prasad, B. V., King, J., Prevelige, P. E., & Chiu, W. (1996). Three-dimensional structure of scaffolding-containing phage p22 procapsids by electron cryo-microscopy. *Journal of Molecular Biology*, 260(1), 85–98.
223. Thuman-Commike, P. A.; Greene, B.; Malinski, J. A.; Burbea, M.; McGough, A.; Chiu, W. & Prevelige Jr, P. E. (1999). Mechanism of scaffolding-directed virus assembly suggested by comparison of scaffolding-containing and scaffolding-lacking P22 procapsids. *Biophysical journal* 1999, 76 (6), 3267-3277.
224. Tishkov, V. I., & Popov, V. O. (2004). Catalytic mechanism and application of formate dehydrogenase. *Biochemistry. Biokhimiia*, 69(11), 1252–1267.
225. Tishkov, V. I. & Popov, V. O. (2006). Protein engineering of formate dehydrogenase. *Biomol Eng* 2006, 23 (2-3), 89-110.
226. Tomczak, J. M., & Węglarz-Tomczak, E. (2019). Estimating kinetic constants in the Michaelis-Menten model from one enzymatic assay using Approximate Bayesian Computation. *FEBS Letters*, 593(19), 2742–2750.
227. Tronchet, M., Balagué, C., Kroj, T., Jouanin, L., & Roby, D. (2010). Cinnamyl alcohol dehydrogenases-C and D, key enzymes in lignin biosynthesis, play an essential role in disease resistance in *Arabidopsis*. *Molecular Plant Pathology*, 11(1), 83–92.
228. Tuan, P. A., Zhao, S., Kim, J. K., Kim, Y. B., Yang, J., Li, C. H., Kim, S.-J., et al. (2014). Riboflavin accumulation and molecular characterization of cDNAs encoding

- bifunctional GTP cyclohydrolase II/3,4-dihydroxy-2-butanone 4-phosphate synthase, lumazine synthase, and riboflavin synthase in different organs of *Lycium chinense* plant. *Molecules* (Basel, Switzerland), 19(11), 17141–17153.
229. Tuma, R.; Parker, M. H.; Weigele, P.; Sampson, L.; Sun, Y.; Krishna, N. R.; Casjens, S.; Thomas Jr, G. J. & Prevelige Jr, P. E. (1998). A helical coat protein recognition domain of the bacteriophage P22 scaffolding protein. *J Mol Biol* 1998, 281 (1), 81-94.
 230. Uchida, M., Klem, M. T., Allen, M., Suci, P., Flenniken, M., Gillitzer, E., Varpness, Z., et al. (2007). Biological Containers: Protein Cages as Multifunctional Nanoplatforms. *Advanced Materials*, 19(8), 1025–1042.
 231. Uchida, M., LaFrance, B., Broomell, C. C., Prevelige, P. E., & Douglas, T. (2015). Higher order assembly of virus-like particles (VLPs) mediated by multi-valent protein linkers. *Small* (Germany), 11(13), 1562–1570.
 232. Uchida, M., McCoy, K., Fukuto, M., Yang, L., Yoshimura, H., Miettinen, H. M., LaFrance, B., et al. (2018). Modular Self-Assembly of Protein Cage Lattices for Multistep Catalysis. *ACS Nano*, 12(2), 942–953.
 233. Vivian, J. T., & Callis, P. R. (2001). Mechanisms of tryptophan fluorescence shifts in proteins. *Biophysical Journal*, 80(5), 2093–2109.
 234. Waghvani, H. K., Uchida, M., Fu, C.-Y., LaFrance, B., Sharma, J., McCoy, K., & Douglas, T. (2020). Virus-Like Particles (VLPs) as a Platform for Hierarchical Compartmentalization. *Biomacromolecules*, 21(6), 2060–2072.
 235. Wang, D., Liu, X., Wei, M., Qian, C., Song, S., Chen, J., Wang, Z., et al. (2020). Rational design of a multi-valent human papillomavirus vaccine by capsomere-hybrid co-assembly of virus-like particles. *Nature Communications*, 11(1), 2841.
 236. Wang, Y., Wang, G., Duan, W.-T., Sun, M.-X., Wang, M.-H., Wang, S.-H., Cai, X.-H., et al. (2020). Self-assembly into virus-like particles of the recombinant capsid protein of porcine circovirus type 3 and its application on antibodies detection. *AMB Express*, 10(1), 3.
 237. Wang, Y.; Uchida, M.; Waghvani, H. K. & Douglas, T. (2020). Synthetic virus-like particles for glutathione biosynthesis. *ACS Synthetic Biology* 2020, 9 (12), 3298-3310.
 238. Waghvani, H. Kumar, M. Uchida, Chi-Yu Fu, B., Jhanvi Sharma, K. McCoy, & T. Douglas (2020). "Virus-Like Particles (VLPs) as a Platform for Hierarchical Compartmentalization." *Biomacromolecules* 21.6 (2020): 2060-072. Web.
 239. Wei, Y., Wahome, N., VanSlyke, G., Whitaker, N., Kumar, P., Barta, M. L., Picking, W. L., et al. (2017). Evaluation of lumazine synthase from *Bacillus anthracis* as a presentation platform for polyvalent antigen display. *Protein Science*, 26(10), 2059–2072.
 240. Weigele, P. R.; Sampson, L.; Winn-Stapley, D. & Casjens, S. R. (2005). Molecular genetics of bacteriophage P22 scaffolding protein's functional domains. *J Mol Biol* 2005, 348 (4), 831-844.
 241. Wilcox, A. E., LoConte, M. A., & Slade, K. M. (2016). Effects of Macromolecular Crowding on Alcohol Dehydrogenase Activity Are Substrate-Dependent. *Biochemistry*, 55(25), 3550–3558.

242. Wilkerson, J. W., Yang, S.-O., Funk, P. J., Stanley, S. K., & Bundy, B. C. (2018). Nanoreactors: Strategies to encapsulate enzyme biocatalysts in virus-like particles. *New Biotechnology*, 44, 59–63.
243. Worsdorfer, B.; Woycechowsky, K. J. & Hilvert, D. (2011). Directed Evolution of a Protein Container. *Science* 2011, 331 (6017), 589-592.
244. Yadav, R. K.; Baeg, J. O.; Oh, G. H.; Park, N. J.; Kong, K. J.; Kim, J.; Hwang, D. W. & Biswas, S. K. (2012). A Photocatalyst-Enzyme Coupled Artificial Photosynthesis System for Solar Energy in Production of Formic Acid from CO₂. *J Am Chem Soc* 2012, 134 (28), 11455-11461.
245. Yang, P., Zhou, R., Kong, C., Fan, L., Dong, C., Chen, J., Hou, X., et al. (2021). Stimuli-Responsive Three-Dimensional DNA Nanomachines Engineered by Controlling Dynamic Interactions at Biomolecule-Nanoparticle Interfaces. *ACS Nano*, 15(10), 16870–16877.
246. Yeates, T. O.; Thompson, M. C. & Bobik, T. A. (2011). The protein shells of bacterial microcompartment organelles. *Current Opinion in Structural Biology* 2011, 21 (2), 223-231.
247. Zandi, R., Dragnea, B., Travesset, A., & Podgornik, R. (2020). On virus growth and form. *Physics Reports*, 847, 1–102.
248. Zeltins, A. (2013). Construction and characterization of virus-like particles: a review. *Molecular Biotechnology*, 53(1), 92–107.
249. Zhang, C., Adera, S., Aizenberg, J., & Chen, Z. (2021). Why Are Water Droplets Highly Mobile on Nanostructured Oil-Impregnated Surfaces? *ACS Applied Materials & Interfaces*, 13(13), 15901–15909.
250. Zhang, K., & Wu, X. Y. (2004). Temperature and pH-responsive polymeric composite membranes for controlled delivery of proteins and peptides. *Biomaterials*, 25(22), 5281–5291.
251. Zhu, R., Li, C., Chen, C., Xing, S., Cai, Y., Zeng, X., & He, L. (2021). Effect of cross-linked enzyme aggregate strategy on characterization of sn-1,3 extracellular lipase from *Aspergillus niger* GZUF36. *Applied Microbiology and Biotechnology*, 105(5), 1925–1941.
252. Zlotnick, A. (2003). Are weak protein–protein interactions the general rule in capsid assembly? *Virology*, 315(2), 269–274.
253. Zlotnick, A. (2005). Theoretical aspects of virus capsid assembly. *Journal of Molecular Recognition*, 18(6), 479–490.
254. Zlotnick, A., Lee, A., Bourne, C. R., Johnson, J. M., Domanico, P. L., & Stray, S. J. (2007). *In vitro* screening for molecules that affect virus capsid assembly (and other protein association reactions). *Nature Protocols*, 2(3), 490–498.